Standard Perturbation Theory in Scale-Dependent Modified Gravity

THESIS

submitted in partial fulfillment of the
requirements for the degree of

MASTER OF SCIENCE
in
PHYSICS

Author :	Anjali Santhosh Madangarli
Supervisor :	Dr Alessandra Silvestri
Co-supervisor :	Stan Verhoeve
Second corrector :	Dr Subodh Patil

Leiden, The Netherlands, April 29, 2026

Standard Perturbation Theory in Scale-Dependent Modified Gravity

Anjali Santhosh Madangarli

Huygens-Kamerlingh Onnes Laboratory, Leiden University
P.O. Box 9500, 2300 RA Leiden, The Netherlands

April 29, 2026

Abstract

The late-time accelerated expansion of the universe remains one of the central problems in modern cosmology. Modified gravity theories offer an alternative to invoking the elusive dark energy to account for this expansion. These modifications introduce an additional degree of freedom that alters the dynamics of gravitational instability on cosmological scales while reproducing a ΛCDM background expansion. In this thesis, we analyse a perturbative framework for studying structure growth within such theories, with a focus on chameleon-screened $f(R)$ gravity. We begin by deriving the fluid equations for cold dark matter within standard perturbation theory. The non-linear mode couplings are encoded in the kernels F_n and G_n, which enter higher-order statistics, like one-loop corrections to the matter power spectrum in the quasi-non-linear regime. We then introduce modified gravity and set up screening mechanisms that suppress EP violations in local high-density environments. Specialising to $f(R)$ gravity, we derive the modified Poisson equation that contains a scale-dependent linear modification and non-linear source terms that are characterised by the interaction coefficients M_1, M_2, and M_3. For the Hu-Sawicki model, we compute the Poisson equation vertices assuming a ΛCDM background and implement a numerical analysis to study their scale and time-dependence. Our results show that GR is recovered at early times, while deviations emerge below the Compton scale. We find that the non-linear vertices dominate close to the Compton crossing and the location and width of this transition depend sensitively on the model parameter f_{R0}. These findings highlight the importance of non-linear corrections and screening effects when modelling structure formation for Stage IV surveys like *Euclid*.

Contents

Chapter 1

Introduction

Einstein's theory of general relativity has withstood thorough experimental scrutiny for over a century, and has emerged as a successful description of gravitational phenomena across different physical regimes. Solar system tests, such as the perihelion precession of Mercury and the Shapiro time delay, and laboratory experiments, including Eötvös-type equivalence principle tests, have confirmed its predictions in the weak field regime with great precision. However, on cosmological scales, the theory remains comparatively less constrained, and it is tested mainly through its role in shaping the growth of structure and expansion history of the universe. In particular, large-scale structure probes gravity on very large scales with low curvature and offers new avenues to study possible deviations from GR.

The main discovery that motivated such an investigation was the late-time accelerated expansion of the universe. Within the framework of general relativity, a seemingly new fluid with a negative equation of state, in the form of the cosmological constant or dynamical dark energy, is required to generate such an expansion [1]. An alternative explanation was that gravity itself was poorly understood on large scales and needed to be modified [2, 3]. While the cosmological constant provides a simple phenomenological description for the acceleration, there is substantial disagreement between the observed and theoretical values of its energy density. Therefore, modified gravity theories remain a compelling alternative for explaining the observed expansion.

From a theoretical perspective, any modification to gravity must introduce new degrees of freedom, the most common ones being scalar fields

[4]. Such modifications affect the growth of cosmological perturbations in the universe. Therefore, the most distinctive signatures of the new degrees of freedom are observed in the growth of cosmic structure, and not on the homogeneous background expansion, which can oftentimes be tuned to mimic ΛCDM in modified gravity models. As a result, it is difficult to distinguish between models of dark energy and modified gravity at the level of background expansion and linear growth.

The non-linear regime of structure formation is hence a powerful observational window for testing gravity on cosmological scales. In theories of modified gravity, the equations that govern the evolution of matter perturbations are altered through modifications to the Poisson equation and the slip between the Newtonian potentials. As highlighted in [3], such modifications lead to scale and time-dependent growth of density perturbations, with an anomalous enhancement occurring within the Compton radius associated with the scalar field [5, 6]. Beyond this radius, gravity reduces to its general relativistic form on sufficiently small scales in dense environments due to screening mechanisms such as chameleon screening [7]. It is important to incorporate screening in such models because solar system tests and fifth-force searches place tight constraints on the presence of additional degrees of freedom and limit any unsuppressed scalar-mediated interactions in high density environments [8, 9]. This permits such models to remain viable in local environments while altering the dynamics of matter perturbations on cosmological scales. Together, these characteristic behaviors allow us to single out intermediate scales, typically of order megaparsec, where we can potentially detect deviations from GR [3].

A particularly well studied class of modified gravity models is $f(R)$ gravity, in which the Einstein-Hilbert action is modified by the addition of a general function of the Ricci scalar. It is seen that suitably chosen $f(R)$ models can reproduce the ΛCDM expansion history while influencing the evolution of perturbations [10]. $f(R)$ theories introduce a scalar degree of freedom whose effective mass depends on the local matter density, thereby demonstrating chameleon screening. Within such theories, the growth of structure is explicitly scale-dependent and is governed by a modified effective Newton's constant [11].

These modifications have measurable consequences on cosmological observables. The matter power spectrum and higher-order statistics are altered due to changes in the linear growth and non-linear mode coupling. Therefore, it is necessary to go beyond linear perturbation theory to accurately capture these effects. The precision demanded by forthcoming

surveys, such as *Euclid*, also motivates the development of more refined perturbative and numerical techniques. As the sensitivity of *Euclid* will extend deep into the quasi-non-linear regime, theoretical modeling must account for non-linear gravitational dynamics, scale-dependent growth, and screening effects [12, 13]. Forecasts indicate that *Euclid* will be capable of distinguishing viable $f(R)$ models from ΛCDM at high statistical significance, provided the theoretical predictions for relevant observables are sufficiently accurate [13].

Therefore, in order to address these challenges, there are stringent demands on the theoretical framework used to interpret large-scale structure data. Perturbative approaches, such as standard perturbation theory and effective field theory methods, depend on the accurate computation of density and velocity kernels that encode mode coupling. Understanding how these kernels are modified by gravity beyond GR is necessary to ensure reliable inference from upcoming data.

The aim of this thesis is to analyse the perturbative framework for studying large scale structure formation in modified gravity. We will particularly focus on $f(R)$ models that exhibit chameleon screening. By deriving and studying the scale and time-dependent perturbative kernels, this work aims to identify signatures of modified gravity in the matter power spectrum beyond the linear order. We particularly focus on the transition between screened and unscreened regimes and the role of modified Poisson equation vertices in implementing screening mechanisms. We also study the dependence of non-linear effects on the model parameters. In doing so, this thesis contributes to the broader effort of building tools capable of interpreting high-precision cosmological data from Stage IV surveys.

The structure of the thesis is as follows. In Chapter 2, we review the fluid description of cold dark matter within the framework of standard perturbation theory. We extend the fluid description to higher orders and study their impact on the matter power spectrum. Chapter 3 introduces modified gravity theories and screening mechanisms, with a particular focus on chameleon screening and its dynamics. In Chapter 4, we take a closer look at $f(R)$ theories, discuss conditions for viability, and study the behavior of perturbations within this theory of gravity. In Chapter 5, we derive the linear and non-linear vertices that enter the modified Poisson equation in the Hu-Sawicki model of $f(R)$ gravity. In Chapter 6, we conduct a numerical analysis of these coefficients, explore their time and scale-independence, and identify regimes that exhibit deviations from GR. Finally, in Chapter 7 we summarize the results and discuss possible direc-

tions for future work.

Chapter 2

Standard Perturbation Theory

Gravitational instability plays a central role in the formation of large-scale structures observed in the universe. In this section, we motivate the use of cosmological perturbation theory in regimes where non-linear contributions become significant. Perturbative solutions are introduced to derive the standard perturbation theory (SPT) kernels that enter the matter power spectrum and higher-order statistics. This will form the foundation for studying the quasi-non-linear and non-linear regime of structure formation in modified gravity models in the later chapters.

2.1 Fluid Description of Cold Dark Matter

In the standard homogeneous and isotropic universe, collisionless dark matter can be modeled as a cold, pressureless fluid, whose dynamics are governed by the Vlasov equation.

2.1.1 Phase-Space Description

Considering that dark matter only interacts gravitationally in an expanding universe, the equation of motion for a collisionless, pressureless fluid with velocity $\mathbf{v}$ and position $\mathbf{r}$ is,

$$\frac{d\mathbf{v}}{dt} = -\frac{\partial\phi}{\partial r}, \tag{2.1}$$

where ϕ is the smooth Newtonian potential sourced by the local mass density $\rho(\mathbf{r})$. The gravitational instability in an expanding universe can be described in terms of the comoving coordinates $\mathbf{x}$, where $\mathbf{r} = a(\tau)\mathbf{x}$, and the conformal time τ ($d\tau = dt/a$). The matter density is expressed in terms of the contrast δ as,

$$\rho(\mathbf{x}, \tau) \equiv \bar{\rho}(\tau)[1 + \delta(\mathbf{x}, \tau)], \tag{2.2}$$

where $\bar{\rho}(\tau)$ denotes the homogeneous background matter density. The particle velocity can be decomposed in the following manner:

$$\mathbf{v}(\mathbf{x}, \tau) \equiv \underbrace{\mathcal{H}(\tau)\,\mathbf{x}}_{\text{homogeneous expansion}} + \underbrace{\mathbf{u}(\mathbf{x}, \tau)}_{\text{peculiar component}}, \tag{2.3}$$

where $\mathcal{H} \equiv d \ln a / d\tau$ is the conformal Hubble expansion rate. Similarly, we can expand the gravitational potential into a homogeneous background component and a fluctuation $\Phi(\mathbf{x}, \tau)$, the latter of which satisfies the Poisson equation,

$$\nabla^2 \Phi(\mathbf{x}, \tau) = \frac{3}{2} \Omega_m(\tau) \mathcal{H}^2(\tau) \delta(\mathbf{x}, \tau), \tag{2.4}$$

where $\Omega_m(\tau)$ is the matter density parameter. The system can be described using the phase-space distribution function $f(\mathbf{x}, \mathbf{p}, \tau)$, where $\mathbf{p} = am\mathbf{u}$ is the comoving momentum. Then the conservation of phase-space density implies that the distribution function f satisfies the Vlasov equation,

$$\frac{df}{d\tau} = \frac{\partial f}{\partial \tau} + \frac{\mathbf{p}}{ma} \cdot \nabla f - am \nabla \Phi \cdot \frac{\partial f}{\partial \mathbf{p}} = 0. \tag{2.5}$$

The intrinsic non-linearity of this equation arises due to its coupling with the gravitational potential through the Poisson equation, making it difficult to solve. However, the combination of the Poisson and Vlasov equations provides a kinetic description for the perturbative approach to cosmic structure formation.

2.1.2 Fluid Equations from the Vlasov Equation

Instead of solving the full phase-space dynamics, we can describe the system in terms of momentum moments, which give rise to fluid variables defined as fields over space. The zeroth moment defines the local mass density as

$$\int d^3\mathbf{p} f(\mathbf{x}, \mathbf{p}, \tau) \equiv \rho(\mathbf{x}, \tau). \tag{2.6}$$

The peculiar velocity $u(\mathbf{x}, \tau)$ is defined by the first moment,

$$\int d^3\mathbf{p} \frac{\mathbf{p}}{am} f(\mathbf{x}, \mathbf{p}, \tau) \equiv \rho(\mathbf{x}, \tau)\mathbf{u}(\mathbf{x}, \tau), \tag{2.7}$$

while the second moment defines the stress tensor $\sigma_{ij}(\mathbf{x}, \tau)$,

$$\int d^3\mathbf{p} \frac{p_i p_j}{a^2 m^2} f(\mathbf{x}, \mathbf{p}, \tau) \equiv \rho(\mathbf{x}, \tau)\mathbf{u}_i(\mathbf{x}, \tau)u_j(\mathbf{x}, \tau) + \sigma_{ij}(\mathbf{x}, \tau). \tag{2.8}$$

Taking moments of the Vlasov equation yields the corresponding fluid equations for these fields. This includes the **continuity equation**, which describes mass conservation, from the zeroth moment,

$$\frac{\partial \delta(\mathbf{x}, \tau)}{\partial \tau} + \nabla \cdot \{[1 + \delta(\mathbf{x}, \tau)]\mathbf{u}(\mathbf{x}, \tau)\} = 0, \tag{2.9}$$

and the **Euler equation**, which describes momentum conservation, from the first moment,

$$\frac{\partial \mathbf{u}(\mathbf{x}, \tau)}{\partial \tau} + \mathcal{H}(\tau)\mathbf{u}(\mathbf{x}, \tau) + \mathbf{u}(\mathbf{x}, \tau) \cdot \nabla \mathbf{u}(\mathbf{x}, \tau) = -\nabla \Phi(\mathbf{x}, \tau) - \frac{1}{\rho}\nabla_j(\rho \sigma_{ij}). \tag{2.10}$$

In the early stages of gravitational instability, it can be assumed that structure formation is driven by matter with negligible velocity dispersions. Therefore, one can set the stress tensor $\sigma_{ij} \approx 0$, which characterises the deviation of particle motions from a single coherent flow. However, this approximation is expected to break down when multi-streams generate non-zero velocity dispersion on sufficiently small scales [14].

Next, we can redefine the variables in terms of the velocity divergence $\theta \equiv \nabla \cdot \mathbf{u}$ and vorticity $\omega \equiv \nabla \times \mathbf{u}$. However, in the pressureless single-stream regime, if absent initially, vorticity is not generated throughout the

evolution. This motivates the irrotational approximation used in standard perturbation theory.

2.2 Cosmological Perturbation Equations in an Expanding Universe

The main assumption underlying perturbation theory is that the density and velocity fields can be expanded about the linear solution and we can treat the variance of the linear fluctuations as a small parameter. This allows us to express the fields as

$$\delta(\mathbf{x},\tau) = \sum_{n=1}^{\infty} \delta^{(n)}(\mathbf{x},\tau), \qquad \theta(\mathbf{x},\tau) = \sum_{n=1}^{\infty} \theta^{(n)}(\mathbf{x},\tau), \tag{2.11}$$

where $\delta^{(1)}$ and $\theta^{(1)}$ are linear in the initial density field, $\delta^{(2)}$ and $\theta^{(2)}$ are quadratic in the initial density field, and so on.

2.2.1 Equations of Motion in Fourier Representation

On sufficiently large scales, cosmological perturbations are statistically homogeneous and isotropic, which allows us to decompose the density and velocity fields into Fourier modes. In this representation, each Fourier mode $\mathbf{k}$ represents a fluctuation with comoving wavelength $\lambda = 2\pi/k$. In the linear regime, a homogeneous (translationally invariant) background implies that each Fourier mode evolves independently. However, when we include non-linear terms, the equations of motion in Fourier space explicitly reveal how different modes couple to each other. Therefore, studying the dynamics in this representation allows us to identify the fundamental mode-coupling structures that govern the non-linear evolution of cosmological perturbations.

In this section, we adopt the following convention for the Fourier transformation of a field $A(\mathbf{x},\tau)$:

$$\tilde{A}(\mathbf{k},\tau) = \int \frac{d^3\mathbf{x}}{(2\pi)^3} \exp(-i\mathbf{k}\cdot\mathbf{x}) A(\mathbf{x},\tau). \tag{2.12}$$

Taking the Fourier transformation of the continuity equation (2.9) and

recalling that $\nabla \cdot \mathbf{u} = \theta$, we obtain,

$$\partial_\tau \delta(\mathbf{k}, \tau) + \theta(\mathbf{k}, \tau) = -\int \frac{d^3\mathbf{x}}{(2\pi)^3} e^{-i\mathbf{k}\cdot\mathbf{x}} \nabla \cdot [\delta(\mathbf{x})\mathbf{u}(\mathbf{x})]. \tag{2.13}$$

Integrating the expression on the right-hand side and assuming that the fields vanish at infinity,

$$\partial_\tau \delta(\mathbf{k}, \tau) + \theta(\mathbf{k}, \tau) = -i\mathbf{k} \int \frac{d^3\mathbf{x}}{(2\pi)^3} e^{-i\mathbf{k}\cdot\mathbf{x}} \delta(\mathbf{x})\mathbf{u}(\mathbf{x}). \tag{2.14}$$

Taking the inverse Fourier transform of the product $\delta(\mathbf{x})\mathbf{u}(\mathbf{x})$ and integrating over comoving space gives

$$\partial_\tau \delta(\mathbf{k}, \tau) + \theta(\mathbf{k}, \tau) = -i\mathbf{k} \int d^3\mathbf{q} d^3\mathbf{p} \delta_D(\mathbf{k} - \mathbf{p} - \mathbf{q}) \tilde{\delta}(\mathbf{p}) \tilde{\mathbf{u}}(\mathbf{q}). \tag{2.15}$$

The irrotational flow approximation ($\nabla \times \mathbf{u} = 0$) in Fourier space implies that the velocity field satisfies $\mathbf{u}(\mathbf{k}) \parallel \mathbf{k}$. This allows us to write

$$\tilde{\mathbf{u}}(\mathbf{k}) = A(\mathbf{k}) \cdot \mathbf{k}, \tag{2.16}$$

where $A(\mathbf{k})$ is some scalar function of the wavenumber $\mathbf{k}$. However, since $\tilde{\theta}(\mathbf{k}) = i\mathbf{k} \cdot \tilde{\mathbf{u}}(\mathbf{k})$, substituting the above expression gives

$$\tilde{\theta} = ik^2 A(\mathbf{k}). \tag{2.17}$$

The velocity field is therefore given by

$$\tilde{\mathbf{u}}(\mathbf{k}) = -\frac{i\tilde{\theta}(\mathbf{k}) \cdot \mathbf{k}}{k^2}. \tag{2.18}$$

Using the above relation to rewrite equation (2.15) and performing a change of integration variables, the expression becomes

$$\partial_\tau \delta(\mathbf{k}, \tau) + \theta(\mathbf{k}, \tau) = -\int d^3\mathbf{p} d^3\mathbf{q} \delta_D(\mathbf{k} - \mathbf{p} - \mathbf{q}) \left[\frac{(\mathbf{q} + \mathbf{p}) \cdot \mathbf{q}}{q^2}\right] \tilde{\delta}(\mathbf{p}) \tilde{\theta}(\mathbf{q}). \tag{2.19}$$

The fundamental non-linear mode couplings in the expression can be

encoded within the so-called α-kernel, which is defined as

$$\alpha(\mathbf{q}, \mathbf{p}) = \frac{(\mathbf{p} + \mathbf{q}) \cdot \mathbf{q}}{q^2}. \tag{2.20}$$

Therefore, the **continuity equation** in Fourier space becomes

$$\boxed{\begin{aligned}\partial_\tau \delta(\mathbf{k}, \tau) + \theta(\mathbf{k}, \tau) = -\int d^3\mathbf{p}\, d^3\mathbf{q}\; \delta_D(\mathbf{k} - \mathbf{p} - \mathbf{q})\, \alpha(\mathbf{q}, \mathbf{p}) \\ \times \tilde{\delta}(\mathbf{p})\, \tilde{\theta}(\mathbf{q})\end{aligned}} \tag{2.21}$$

Similarly, taking the divergence of the Euler equation (2.10) yields

$$\partial_\tau \theta + \mathcal{H}\theta + \nabla \cdot \big[(\mathbf{u} \cdot \nabla)\mathbf{u}\big] = -\nabla^2 \Phi. \tag{2.22}$$

Upon substituting the Poisson equation and taking the Fourier transform, the equations become

$$\partial_\tau \tilde{\theta}(\mathbf{k}, \tau) + \mathcal{H}\tilde{\theta}(\mathbf{k}, \tau) + \frac{3}{2}\Omega_m \mathcal{H}^2 \tilde{\delta}(\mathbf{k}, \tau) = -\mathcal{F}\{\nabla \cdot [(\mathbf{u} \cdot \nabla)\mathbf{u}]\}. \tag{2.23}$$

To obtain the Fourier transform of the non-linear term on the right-hand side of the above expression, we use the following identity,

$$(\mathbf{u} \cdot \nabla)\mathbf{u} = \nabla\left(\frac{u^2}{2}\right) + (\nabla \times \mathbf{u}) \times \mathbf{u}. \tag{2.24}$$

Combined with the assumption of an irrotational fluid, this identity simplifies the non-linear terms, and gives the equation

$$\begin{aligned}\partial_\tau \tilde{\theta}(\mathbf{k}, \tau) + \mathcal{H}\tilde{\theta}(\mathbf{k}, \tau) + \frac{3}{2}\Omega_m \mathcal{H}^2 \tilde{\delta}(\mathbf{k}, \tau) = \frac{1}{2}\int d^3\mathbf{p}\, d^3\mathbf{q}\; (\mathbf{p} + \mathbf{q})^2 \\ \times \delta_D(\mathbf{p} + \mathbf{q} - \mathbf{k}) \tilde{u}(\mathbf{p})\, \tilde{u}(\mathbf{q}).\end{aligned} \tag{2.25}$$

Using equation (2.18) allows the velocity field to be re-expressed in

terms of its divergence, resulting in

$$\partial_\tau \tilde{\theta}(\mathbf{k},\tau) + \mathcal{H}\tilde{\theta}(\mathbf{k},\tau) + \frac{3}{2}\Omega_m \mathcal{H}^2 \tilde{\delta}(\mathbf{k},\tau) = -\frac{1}{2}\int d^3\mathbf{p}\, d^3\mathbf{q}\; \delta_D(\mathbf{p}+\mathbf{q}-\mathbf{k}) \times \left[\frac{(\mathbf{p}+\mathbf{q})^2(\mathbf{q}\cdot\mathbf{p})}{q^2 p^2}\right] \tilde{\theta}(\mathbf{p})\tilde{\theta}(\mathbf{q}). \tag{2.26}$$

Therefore, the second fundamental non-linear mode coupling kernel $\beta(\mathbf{q},\mathbf{p})$ is defined as

$$\beta(\mathbf{q},\mathbf{p}) = \frac{(\mathbf{q}+\mathbf{p})^2 \mathbf{q}\cdot\mathbf{p}}{2q^2p^2}. \tag{2.27}$$

The **Euler equation** then reads

$$\boxed{\partial_\tau \tilde{\theta}(\mathbf{k},\tau) + \mathcal{H}\tilde{\theta}(\mathbf{k},\tau) + \frac{3}{2}\Omega_m \mathcal{H}^2 \tilde{\delta}(\mathbf{k},\tau) = -\int d^3\mathbf{p}\, d^3\mathbf{q}\; \delta_D(\mathbf{p}+\mathbf{q}-\mathbf{k}) \times \beta(\mathbf{q},\mathbf{p})\, \tilde{\theta}(\mathbf{p})\tilde{\theta}(\mathbf{q})} \tag{2.28}$$

Therefore, the α and β-kernels arise due to the non-linear terms of the continuity and Euler equations and encode the non-linearity of the evolution. The dynamical evolution of $\tilde{\delta}(\mathbf{k},\tau)$ and $\tilde{\theta}(\mathbf{k},\tau)$ is determined by the mode couplings of fields at all wavevectors $\mathbf{p}$ and $\mathbf{q}$, which satisfy $\mathbf{k} = \mathbf{q} + \mathbf{p}$, as required by translational invariance in a homogeneous universe.

Summary: Equations of Motion and Mode-Coupling Kernels

The evolution of the density contrast δ and velocity divergence θ in Fourier space is governed by

$$\partial_\tau \delta(\mathbf{k},\tau) + \theta(\mathbf{k},\tau) = -\int d^3\mathbf{p}\, d^3\mathbf{q}\; \delta_D(\mathbf{p}+\mathbf{q}-\mathbf{k})\, \alpha(\mathbf{p},\mathbf{q})\, \theta(\mathbf{p},\tau)\, \delta(\mathbf{q},\tau), \tag{2.29}$$

$$\partial_\tau \theta(\mathbf{k},\tau) + \mathcal{H}\theta(\mathbf{k},\tau) + \frac{3}{2}\Omega_m \mathcal{H}^2 \delta(\mathbf{k},\tau) = -\int d^3\mathbf{p}\, d^3\mathbf{q}\; \delta_D(\mathbf{p}+\mathbf{q}-\mathbf{k})\, \beta(\mathbf{p},\mathbf{q})\, \theta(\mathbf{p},\tau)\, \theta(\mathbf{q},\tau), \tag{2.30}$$

where the mode-coupling kernels are given by

$$\alpha(\mathbf{q},\mathbf{p}) = \frac{(\mathbf{p}+\mathbf{q})\cdot\mathbf{p}}{p^2}, \tag{2.31}$$

$$\beta(\mathbf{q},\mathbf{p}) = \frac{(\mathbf{p}+\mathbf{q})^2\,(\mathbf{p}\cdot\mathbf{q})}{2\,p^2 q^2}. \tag{2.32}$$

2.3 Higher-Order Solutions in Einstein-de Sitter Cosmology

To illustrate the general method for solving the fluid equations, we consider the case of Einstein-de Sitter Cosmology with $\Omega_m = 1$ and $\Omega_\Lambda = 0$. To begin, we use the following perturbative expansions:

$$\tilde{\delta}(\mathbf{k},\tau) = \sum_{n=1}^{\infty} a^n(\tau)\delta_n(\mathbf{k}), \qquad \tilde{\theta}(\mathbf{k},\tau) = -\mathcal{H}(\tau)\sum_{n=1}^{\infty} a^n(\tau)\theta_n(\mathbf{k}). \tag{2.33}$$

Here, the time dependence factors out as powers of the scale factor $a(\tau)$. This implies that the time evolution is universal while all the spatial/mode structure is encoded within the fucntional forms of δ_n and θ_n. The equations of motion determine the higher-order contributions to $\delta(\mathbf{k},\tau)$ and $\theta(\mathbf{k},\tau)$ in terms of convolutions of the linear density field. Consequently, the general solutions take the form,

$$\delta_n(\mathbf{k}) = \int d^3\mathbf{q}_1 ... \int d^3\mathbf{q}_n \delta_D(\mathbf{k} - \mathbf{q}_{1..n}) F_n(\mathbf{q}_1, ..., \mathbf{q}_n) \delta_1(\mathbf{q}_1)..\delta_1(\mathbf{q}_n) \quad (2.34)$$

$$\theta_n(\mathbf{k}) = -\int d^3\mathbf{q}_1 ... \int d^3\mathbf{q}_n \delta_D(\mathbf{k} - \mathbf{q}_{1..n}) G_n(\mathbf{q}_1, ..., \mathbf{q}_n) \delta_1(\mathbf{q}_1)..\delta_1(\mathbf{q}_n). \quad (2.35)$$

Here, F_n and G_n are homogeneous functions of degree zero, and are constructed using the fundamental mode coupling functions discussed earlier.

Substituting the perturbative expansions from equation (2.33) within the continuity equation (2.21) yields

$$\sum_{n=1}^{\infty} \dot{a}(\tau) a^{n-1} [n\delta_n(\mathbf{k}) + \theta_n(\mathbf{k})] = -\int d^3\mathbf{k}_1 \int d^3\mathbf{k}_2 \delta_D(\mathbf{k}_1 + \mathbf{k}_2 - \mathbf{k}) \alpha(\mathbf{k}_1, \mathbf{k}_2) \times \sum_{m=1}^{n-1} \sum_{n=2}^{\infty} \dot{a}(\tau) a^{n-1}(\tau) \theta_m(\mathbf{k}_1) \delta_{n-m}(\mathbf{k}_2). \quad (2.36)$$

Comparing the coefficients of $\dot{a}(\tau)a^{n-1}$, thereby isolating the n$^{\text{th}}$-order contribution of the series, gives

$$n\delta_n(\mathbf{k}) + \theta_n(\mathbf{k}) = -\int d^3\mathbf{k_1} \int d^3\mathbf{k_2} \delta_D(\mathbf{k}_1 + \mathbf{k}_2 - \mathbf{k}) \times \alpha(\mathbf{k}_1, \mathbf{k}_2) \sum_{m=1}^{n-1} \theta_m(\mathbf{k}_1) \delta_{n-m}(\mathbf{k}_2). \quad (2.37)$$

Similarly, in the case of the Euler equation (2.28), isolating the n$^{\text{th}}$-order contribution of the series yields

$$\frac{3}{2}\delta_n(\mathbf{k}) + \left(n + \frac{1}{2}\right)\theta_n(\mathbf{k}) = -\int d^3\mathbf{k_1}\int d^3\mathbf{k_2}\delta_D(\mathbf{k}_1 + \mathbf{k}_2 - \mathbf{k}) \times\beta(\mathbf{k}_1, \mathbf{k}_2)\sum_{m=1}^{n-1}\theta_m(\mathbf{k}_1)\theta_{n-m}(\mathbf{k}_2). \tag{2.38}$$

Introducing the definitions

$$n\delta_n(\mathbf{k}) + \theta_n(\mathbf{k}) = A_n(\mathbf{k}), \qquad \frac{3}{2}\delta_n(\mathbf{k}) + \left(n + \frac{1}{2}\right)\theta_n(\mathbf{k}) = B_n(\mathbf{k}), \tag{2.39}$$

allows us to express δ_n and θ_n as a linear combination of A_n and B_n as follows:

$$\delta_n(\mathbf{k}) = \frac{(2n+1)A_n(\mathbf{k}) - 2B_n(\mathbf{k})}{n(2n+1) - 3}, \qquad \theta_n(\mathbf{k}) = \frac{2nB_n(\mathbf{k}) - 3A_n(\mathbf{k})}{(2n+3)(n-1)}. \tag{2.40}$$

Using an inductive ansatz, it is possible to show that for all orders n, there exist F_n and G_n that satisfy the equations (2.34) and (2.35). The proof proceeds as follows:

- $n = 1$**:** $F_1(\mathbf{q}_1) = 1$ and $G_1(\mathbf{q}_2) = 1$
  Then $\delta_1(\mathbf{k}) = \int d^3\mathbf{q}_1\delta_D(\mathbf{q}_1 - \mathbf{k})\delta_1(\mathbf{q}_1) = \delta_1(\mathbf{k})$
  and $\theta_1(\mathbf{k}) = -\int d^3\mathbf{q}_1\delta_D(\mathbf{q}_1 - \mathbf{k})\delta_1(\mathbf{q}_1) = -\delta_1(\mathbf{k})$
  Therefore, the base case is satisfied.
- $n \neq 1$**:** We begin by assuming that equations (2.34) and (2.35) hold for all orders n. Substituting the corresponding expansions of δ_n and θ_n into the definitions of A_n and B_n yields:

$$\begin{aligned} A_n(\mathbf{k}) &= \int d^3\mathbf{q}_1...d^3\mathbf{q}_n\delta_D(\mathbf{q}_1 + \mathbf{q}_2 + ... + \mathbf{q_n} - \mathbf{k})\tilde{A}_n(\mathbf{q}_1, ..., \mathbf{q}_n) \\ &\quad\times\delta_1(\mathbf{q}_1)...\delta_1(\mathbf{q}_n) \\ B_n(\mathbf{k}) &= -\int d^3\mathbf{q}_1...d^3\mathbf{q}_n\delta_D(\mathbf{q}_1 + \mathbf{q}_2 + ... + \mathbf{q_n} - \mathbf{k})\tilde{B}_n(\mathbf{q}_1, ..., \mathbf{q}_n) \\ &\quad\times\delta_1(\mathbf{q}_1)...\delta_1(\mathbf{q}_n) \end{aligned} \tag{2.41}$$

where $\tilde{A}_n$ and $\tilde{B}_n$ are,

$$\tilde{A}_n(\mathbf{q}_1, ..., \mathbf{q}_n) = \sum_{m=1}^{n-1} \alpha(\mathbf{q}_1 + ... + \mathbf{q}_m, \mathbf{q}_{m+1} + ... + \mathbf{q}_n) G_m(\mathbf{q}_1, ..., \mathbf{q}_m) \times F_{n-m}(\mathbf{q}_{m+1}, ..., \mathbf{q}_n)$$
$$\tilde{B}_n(\mathbf{q}_1, ..., \mathbf{q}_n) = \sum_{m=1}^{n-1} \beta(\mathbf{q}_1 + ... + \mathbf{q}_m, \mathbf{q}_{m+1} + ... + \mathbf{q}_n) G_m(\mathbf{q}_1, ..., \mathbf{q}_m) \times G_{n-m}(\mathbf{q}_{m+1}, ..., \mathbf{q}_n) \tag{2.42}$$

Substituting the expressions for A_n and B_n back into the relations derived in equation (2.40), and comparing with the general forms of solutions in (2.34) and (2.35) gives the expressions for F_n and G_n as

$$F_n(\mathbf{q}_1, ..., \mathbf{q}_n) = \sum_{m=1}^{n-1} \frac{G_m(\mathbf{q}_1, ..., \mathbf{q}_m)}{(2n+3)(n-1)} [(2n+1)\alpha(\mathbf{k}_1, \mathbf{k}_2) F_{n-m}(\mathbf{q}_{m+1}, ..., \mathbf{q}_n) + 2\beta(\mathbf{k}_1, \mathbf{k}_2) G_{n-m}(\mathbf{q}_{m+1}, ..., \mathbf{q}_n)] \tag{2.43}$$

$$G_n(\mathbf{q}_1, ..., \mathbf{q}_n) = \sum_{m=1}^{n-1} \frac{G_m(\mathbf{q}_1, ..., \mathbf{q}_m)}{(2n+3)(n-1)} [2n\beta(\mathbf{k}_1, \mathbf{k}_2) G_{n-m}(\mathbf{q}_{m+1}, ..., \mathbf{q}_n) + 3\alpha(\mathbf{k}_1, \mathbf{k}_2) F_{n-m}(\mathbf{q}_{m+1}, ..., \mathbf{q}_n)]. \tag{2.44}$$

Therefore, F_n and G_n are kernel functions, which can be computed iteratively and describe how Fourier modes couple together through nonlinear gravitational evolution. They can be represented diagrammatically by the vertex shown in Figure (2.1).

One of the key ideas of SPT is how the F_n and G_n kernel functions can be used to construct higher-order statistics and corrections to the theory. As a consequence, the kernels F_2 and F_3 enter the one-loop matter power spectrum and will be discussed further in the next section.

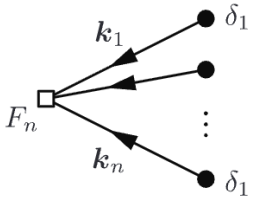

$$\equiv \quad F_n(\boldsymbol{k}_1, \cdots, \boldsymbol{k}_n)\,(2\pi)^3 \delta_D\big(\boldsymbol{k} - \boldsymbol{k}_{1\ldots n}\big)\ .$$

Figure 2.1: *Diagrammatic representation of the n^{th}-order mode-coupling vertex F_n arising from SPT. The figure illustrates how n incoming Fourier modes $\mathbf{k}_1, ..., \mathbf{k}_n$ couple to give a single outgoing mode $\mathbf{k}$, with the conservation of co-moving wave-vectors enforced by the Dirac delta function [15].*

2.4 Power Spectrum Beyond the Linear Order

The statistical properties of a Gaussian density field in Fourier space are completely characterised by its power spectrum (or two-point correlation function), which is defined as

$$\langle \tilde{\delta}(\mathbf{k}, \tau) \tilde{\delta}(\mathbf{k}', \tau) \rangle_c = \delta_D(\mathbf{k} + \mathbf{k}') P(k, \tau). \tag{2.45}$$

However, when the evolution of gravitational instability is non-linear, the mode couplings introduce non-Gaussianities, requiring higher-order perturbation theory to completely characterise the density fields.

2.4.1 Tree-Level Contribution

At leading order, the density contrast δ evolves linearly and takes the form

$$P^{(0)}(k, \tau) = D_+^2(\tau) P_L(k), \tag{2.46}$$

where $D_+(\tau)$ is the linear growth factor while P_L represents the initial (linear) power spectrum. This contribution is called the tree-level or zero-loop power spectrum.

2.4.2 One-Loop Corrections

One-loop perturbation theory describes the initial effects of mode coupling in the evolution of the power spectrum and provides quantitative estimates of where tree-level PT breaks down during the transition to nonlinear regimes. Expanding up to the cubic order in the linear density field gives the one-loop power spectrum,

$$P(k,\tau) = \underbrace{P^{(0)}(k,\tau)}_{\text{linear (tree level)}} + \underbrace{P^{(1)}(k,\tau)}_{\text{one-loop correction}} + ... \tag{2.47}$$

The one-loop contribution can be further expanded as

$$P^{(1)}(k,\tau) = P_{22}(k,\tau) + P_{13}(k,\tau). \tag{2.48}$$

As we can see from Figure (2.2), the term P_{22} arises from the correlations of second-order density perturbations, while P_{13} encodes the coupling between the first and third-order perturbations. Their respective computations are discussed below.

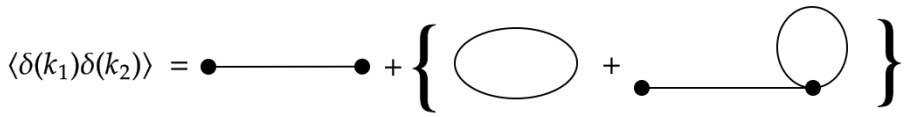

Figure 2.2: *Diagrammatic representation of the matter power spectrum at one-loop order. The first term represents the tree-level contribution* $(P^{(0)})$*, while the rest arise from the loop corrections due to mode-coupling* (P_{22}) *and propagator renormalisation* (P_{13}) *respectively.*

Recalling the general forms of expressions for δ_n from equation (2.34), the second-order contribution is given as

$$\delta^{(2)}(\mathbf{k}) = \int d^3\mathbf{q}_1 d^3\mathbf{q}_2 \delta_D(\mathbf{k}-\mathbf{q}_1-\mathbf{q}_2) F_2^{(s)}(\mathbf{q}_1,\mathbf{q}_2)\delta_1(\mathbf{q}_1)\delta_1(\mathbf{q}_2). \tag{2.49}$$

Plugging this into the definition of $P_{22} = \langle \delta^{(2)}(\mathbf{k})\delta^{(2)}(\mathbf{k}')\rangle$, we get:

$$\langle \delta^{(2)}(\mathbf{k})\delta^{(2)}(\mathbf{k}')\rangle = \int d^3\mathbf{q}_1 d^3\mathbf{q}_2 d^3\mathbf{p}_1 d^3\mathbf{p}_2 \delta_D(\mathbf{k}-\mathbf{q}_1-\mathbf{q}_2)\delta_D(\mathbf{k}'-\mathbf{p}_1-\mathbf{p}_2) \times F_2^{(s)}(\mathbf{q}_1,\mathbf{q}_2)F_2^{(s)}(\mathbf{p}_1,\mathbf{p}_2)\langle \delta_{q_1}\delta_{q_2}\delta_{p_1}\delta_{p_2}\rangle. \tag{2.50}$$

Applying Wick's theorem for a four-point function, the following pairings are possible:

$$\langle \delta_{q_1}\delta_{q_2}\delta_{p_1}\delta_{p_2}\rangle = \underbrace{\langle \delta_{q_1}\delta_{q_2}\rangle\langle \delta_{p_1}\delta_{p_2}\rangle}_{\text{(i)}} + \underbrace{\langle \delta_{q_1}\delta_{p_1}\rangle\langle \delta_{q_2}\delta_{p_2}\rangle}_{\text{(ii)}} + \underbrace{\langle \delta_{q_1}\delta_{p_2}\rangle\langle \delta_{q_2}\delta_{p_1}\rangle}_{\text{(iii)}}. \tag{2.51}$$

Since (i) enforces a zero external momentum, it can be dropped in the case of the connected power spectrum when $k \neq 0$. Using the definition $\langle \delta^{(1)}(\mathbf{a})\,\delta^{(1)}(\mathbf{b})\rangle = \delta_D(\mathbf{a}+\mathbf{b})\,P_L(a)$, the contribution of term (ii) to the integral in equation (2.50) can be expressed as

$$\mathcal{I}_{ii} = \int d^3\mathbf{q}_1 d^3\mathbf{q}_2 d^3\mathbf{p}_1 d^3\mathbf{p}_2 \delta_D(\mathbf{k}-\mathbf{q}_1-\mathbf{q}_2)\delta_D(\mathbf{k}'-\mathbf{p}_1-\mathbf{p}_2) \times F_2^{(s)}(\mathbf{q}_1,\mathbf{q}_2)F_2^{(s)}(\mathbf{p}_1,\mathbf{p}_2) \times \delta_D(\mathbf{p}_1+\mathbf{q}_1)P_L(q_1) \times \delta_D(\mathbf{q}_2+\mathbf{p}_2)P_L(q_2). \tag{2.52}$$

Integrating over $\mathbf{p}_1$ and $\mathbf{p}_2$ reduces the expression to

$$\mathcal{I}_{ii} = \int d^3\mathbf{q}_1 d^3\mathbf{q}_2 \delta_D(\mathbf{k}-\mathbf{q}_1-\mathbf{q}_2)\delta_D(\mathbf{k}'+\mathbf{q}_1+\mathbf{q}_2) \times F_2^{(s)}(\mathbf{q}_1,\mathbf{q}_2)F_2^{(s)}(-\mathbf{q_1},-\mathbf{q_2}) \times P_L(q_1)P_L(q_2). \tag{2.53}$$

Since the symmetrised second-order kernels are homogeneous to degree zero, they satisfy $F_2^{(s)}(\mathbf{q}_1,\mathbf{q}_2) = F_2^{(2)}(-\mathbf{q}_1,-\mathbf{q}_2)$. Further, upon relabeling the integration variables and integrating over $\mathbf{q}_2$, we obtain

$$\mathcal{I}_{ii} = \delta_D(\mathbf{k}+\mathbf{k}') \int d^3\mathbf{q}(F_2^{(s)}(|\mathbf{k}-\mathbf{q}|,\mathbf{q}))^2 P_L(\mathbf{q}). \tag{2.54}$$

Similarly, the contribution from the third term (iii) of equation (2.51) to the integral in (2.50) can also be written as

$$\mathcal{I}_{iii} = \delta_D(\mathbf{k}+\mathbf{k}') \int d^3\mathbf{q} (F_2^{(s)}(|\mathbf{k}-\mathbf{q}|,\mathbf{q}))^2 P_L(\mathbf{q}). \tag{2.55}$$

Therefore, equation (2.50) reduces to,

$$\langle \delta^{(2)}(\mathbf{k})\delta^{(2)}(\mathbf{k}')\rangle = 2\delta_D(\mathbf{k}+\mathbf{k}') \int d^3\mathbf{q} [F_2^{(s)}(|\mathbf{k}-\mathbf{q}|,\mathbf{q})]^2 P_L(q) P_L(|\mathbf{k}-\mathbf{q}|) \tag{2.56}$$

However, by definition, $\langle \delta^{(2)}(\mathbf{k})\delta^{(2)}(\mathbf{k}')\rangle = \delta_D(\mathbf{k}+\mathbf{k}')P_{22}(k)$. Therefore, through comparison, the P_{22} contribution to the one-loop power spectrum is derived as

$$P_{22}(k) = 2\int d^3\mathbf{q} [F_2^{(s)}(|\mathbf{k}-\mathbf{q}|,\mathbf{q})]^2 P_L(q) P_L(|\mathbf{k}-\mathbf{q}|). \tag{2.57}$$

This contribution is positive-definite and characterises how power is transferred between modes due to non-linear interactions.

Similarly, using the definition of $P_{13} = \langle \delta^{(1)}(\mathbf{k})\delta^{(3)}(\mathbf{k}')\rangle$ yields

$$\begin{aligned}\langle \delta^{(1)}(\mathbf{k})\delta^{(3)}(\mathbf{k}')\rangle = \int d^3\mathbf{q}_1 d^3\mathbf{p}_1 d^3\mathbf{p}_2 d^3\mathbf{p}_3 \delta_D(\mathbf{k}-\mathbf{q}_1)\delta_D(\mathbf{k}'-\mathbf{p}_1-\mathbf{p}_2-\mathbf{p}_3) \\ \times F_1^{(s)}(\mathbf{q}_1) F_3^{(s)}(\mathbf{p}_1,\mathbf{p}_2,\mathbf{p}_3)\langle \delta_{q_1}\delta_{p_1}\delta_{p_2}\delta_{p_3}\rangle.\end{aligned} \tag{2.58}$$

Integrating over $\mathbf{q}_1$ and recalling that $F_1^{(s)} = 1$, the integral reduces to

$$\begin{aligned}\langle \delta^{(1)}(\mathbf{k})\delta^{(3)}(\mathbf{k}')\rangle = \int d^3\mathbf{p}_1 d^3\mathbf{p}_2 d^3\mathbf{p}_3 \delta_D(\mathbf{k}'-\mathbf{p}_1-\mathbf{p}_2-\mathbf{p}_3) \\ \times F_3^{(s)}(\mathbf{p}_1,\mathbf{p}_2,\mathbf{p}_3)\langle \delta_k\delta_{p_1}\delta_{p_2}\delta_{p_3}\rangle.\end{aligned} \tag{2.59}$$

Using Wick's theorem and following a similar analysis as before, the P_{13} contribution to the one-loop power spectrum is obtained as

$$P_{13}(\mathbf{k}) = 6 \int d^3\mathbf{q} F_3^{(s)}(\mathbf{k}, \mathbf{q}, -\mathbf{q}) P_L(k) P_L(q). \tag{2.60}$$

Unlike P_{22}, this contribution is in general negative and does not describe mode-coupling. Depending on the form of the initial power spectrum P_L, P_{13} can suppress power on quasi-linear scales leading to effects of previrialisation, which is when small density fluctuations experience non-radial motions and tidal interactions, causing their gravitational collapse [16].

2.4.3 Diagrammatic Representation

The two contributions P_{22} and P_{13} correspond to the diagrams shown in Figure (2.3), where the vertices represent the mode-coupling kernels and the internal lines represents to the linear power spectrum.

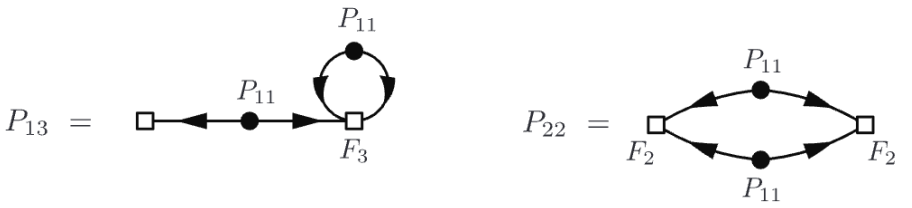

Figure 2.3: *Diagrammatic representation of the one-loop contributions to the matter power spectrum: P_{22} (right) and P_{13} (left). The P_{13} term arises from the coupling between a linear and a third-order perturbation, and P_{22} represents the correlation of two second-order perturbations of the density field. [15].*

Therefore, the kernels F_2 and F_3 play an important role in determining the leading non-linear corrections to the power spectrum. Their explicit form influences the sign and scale-dependence of the one-loop contributions. Each diagram corresponds to an integral over internal momenta.

This diagrammatic representation provides a compact way to study the non-linear corrections to the correlation functions. It is also useful for assessing the infrared and ultraviolet behavior of loop integrals and for understanding how different interactions contribute to the observables, such as the power spectrum [17]. As seen from Figure (2.3), P_{22} comes from the correlation between two second-order density perturbations and represents the simplest irreducible mode-mode coupling. In contrast, P_{13} arises from the coupling between one linear mode and one cubic pertur-

bation, and encodes the self-energy correction that renormalises the linear density propagator [18].

Chapter 3

Modified Gravity and Screening Mechanisms

This chapter introduces the general principles behind theories of modified gravity and provides the physical motivation for screening mechanisms. In particular, we will study chameleon screening, in which the additional degree of freedom is environment-dependent, thereby allowing for the recovery of general relativity in high-density regions.

3.1 Modified Gravity

General relativity has had extraordinary success in making predictions about fundamental physics that have been confirmed through experiments and observations, such as the precession of Mercury perihelion with high precision. In principle, GR is a geometric theory for gravity, in which the spacetime curvature is determined by the energy, momentum, and stress of matter and radiation through the Einstein field equations.

Despite these successes, there are compelling observational and theoretical reasons to consider possible extensions or modifications to general relativity. One such motivation comes from CMB, Type Ia supernovae, and large-scale structure observations that confirm the universe is currently undergoing a period of accelerated expansion. Within general relativity, this expansion is accounted for by introducing a cosmological constant or a dark energy component with a negative equation of state. However, there is substantial disagreement between the observed value of the vac-

uum (cosmological constant) energy density and that predicted theoretically by quantum field theory, which gives rise to the cosmological constant problem [19, 20]. From a theoretical standpoint, general relativity is not perturbatively renormalisable and can be considered as a low-energy effective theory, which indicates the need for extensions or new degrees of freedom at higher energies [21].

This has led to the development of modified gravity theories. Most modified gravity models retain the geometric foundation of GR and extend the gravitational action by introducing additional dynamical fields or geometric invariants. This can be done in a multitude of ways, some of which include theories with higher-order curvature terms in the action, non-Christoffel connections, or even formulating models in higher dimensions [22]. Among these different theories, scalar-tensor theories are particularly important. In such theories, gravitational interactions are governed by both the metric tensor and a scalar degree of freedom that couples to the curvature scalar. In general, the action can be written as a sum of the gravitational piece, a scalar piece, and a pure matter piece [22],

$$S = S_{f_R} + S_\lambda + S_M. \tag{3.1}$$

Depending on the choice of coupling functions, these theories encompass a wide range of modified gravity models, including Brans-Dicke gravity. An important subset of scalar-tensor theories is $f(R)$ gravity, where the Ricci scalar R in the Einstein-Hilbert action is replaced by a general function $f(R)$. Such modifications introduce scale and environment-dependent effects that are not observed in GR.

One of the main challenges for modified gravity theories is satisfying local gravity tests. Since precision measurements in the solar system place extremely tight constraints on deviations from GR [23], any additional degree of freedom must be suppressed in local environments. This is achieved through screening mechanisms, such as chameleon and Vainshtein screening, which suppresses deviation from GR in high-density or high-curvature environments. Screening mechanisms will be discussed in greater detail in the following sections.

3.2 Screening Mechanisms

Observations from Type Ia supernovae and CMB anisotropies indicate that the universe is currently dominated by a dark energy component. While the cosmological constant provides an adequate phenomenological description, more general models of gravity explain dark energy and the late-time acceleration of the universe through a dynamical scalar field. However, for such a field to remain dynamical today, its corresponding mass must be of order H_0 [24].

Scalar fields that are effectively massless on scales of the solar system mediate long-range forces and lead to violations of the Equivalence Principle, which is tightly constrained through astrophysical and laboratory tests [25]. The fields couple to matter with gravitational strength, leading to phenomenological inconsistencies unless their effects are suppressed on these scales. Screening mechanisms reconcile the cosmological implications for such a scalar degree of freedom with stringent local tests of gravity.

3.2.1 Chameleon Screening

Chameleon screening achieves this reconciliation by ensuring that the scalar field acquires a mass whose magnitude depends on the local matter density. In regions of high density, such as the solar system, the associated mass becomes large, causing the force it mediates to become short-ranged and making it unobservable. In contrast, in low-density regions, the force becomes long-ranged and can influence cosmological dynamics [7].

The action governing the dynamics of such a model in the Einstein frame is given by [7]

$$S = \underbrace{\int d^4x\sqrt{-g}\left\{\frac{M_{Pl}^2}{2}\mathcal{R} - \frac{1}{2}(\partial\phi)^2 - V(\phi)\right\}}_{\text{scalar field action}} - \underbrace{\int d^4x\mathcal{L}_m(\psi_m^{(i)}, g_{\mu\nu}^{(i)})}_{\text{matter action}}, \quad (3.2)$$

where $M_{Pl} = (8\pi G)^{-1/2}$ is the reduced Planck mass and the matter fields $\psi_m^{(i)}$ couple to the scalar field by the conformal rescaling,

$$g_{\nu\mu}^{(i)} = e^{2\beta_i\phi/M_{Pl}}g_{\mu\nu}. \quad (3.3)$$

Here, β_i denote dimensionless coupling constants that need not be extremely small; they can be of order unity in their coupling to matter. It is assumed that different matter fields $\psi_m^{(i)}$ do not interact with each other. Further, a runaway potential $V(\phi)$ is assumed which is monotonically decreasing and satisfies the following conditions:

$$\lim_{\phi\to\infty} V(\phi) = 0, \qquad \lim_{\phi\to\infty} \frac{V_{,\phi}}{V} = 0, \qquad \lim_{\phi\to\infty} \frac{V_{,,\phi}}{V_{,\phi}} = 0, \tag{3.4}$$

$$\lim_{\phi\to 0} V(\phi) = \infty, \qquad \lim_{\phi\to 0} \frac{V_{,\phi}}{V} = \infty, \qquad \lim_{\phi\to 0} \frac{V_{,,\phi}}{V_{,\phi}} = \infty. \tag{3.5}$$

An example of such a runaway potential would be the inverse power-law potential

$$V(\phi) = \frac{M^{4+n}}{\phi^n}. \tag{3.6}$$

If the stress-energy tensor for the i$^{\text{th}}$ type of matter is

$$T^{(i)}_{\mu\nu} = \frac{2}{\sqrt{-g^{(i)}}} \frac{\delta \mathcal{L}_m}{\delta g^{\mu\nu}_{(i)}}, \tag{3.7}$$

the equation of motion can be derived by varying the action with respect to the scalar field ϕ. Varying the scalar field part of the action yields

$$\delta S_\phi = \int d^4x \sqrt{-g} (\nabla_\mu \nabla^\mu \phi) \delta\phi. \tag{3.8}$$

For the matter action part, however, there is only an implicit ϕ-dependence in $g^{(i)}_{\mu\nu}$ which arises due to the conformal rescaling. Therefore, the varied action becomes

$$\delta S^{(i)}_m = \int d^4x \sqrt{-g^{(i)}} \frac{\beta_i}{M_{Pl}} g^{(i)}_{\mu\nu} T^{(i)\mu\nu} \delta\phi. \tag{3.9}$$

However, for non-relativistic matter $g^{(i)}_{\mu\nu} T^{(i)\mu\nu} \approx -\tilde{\rho}_i$, where $\tilde{\rho}_i$ is the energy density. Furthermore, $\tilde{\rho}_i$ is not conserved in the Einstein frame, and therefore it is convenient to use an alternate energy density $\rho_i = \tilde{\rho}_i e^{3\beta_i \phi / M_{Pl}}$.

Since $\delta S_\phi + \delta S_m = 0$ for arbitrary $\delta\phi$, the equation of motion is obtained as

$$\boxed{\Box\phi = V_{,\phi} + \sum_i \frac{\beta_i}{M_{Pl}} \rho_i e^{\beta_i \phi / M_{Pl}}} \tag{3.10}$$

From the right-hand side of equation (3.10), it is evident that the dynamics of the scalar field does not just depend on the runaway potential $V(\phi)$, but also on an additional density-dependent term. Therefore, the effective potential can be written as

$$V_{eff}(\phi) = V(\phi) + \sum_i \rho_i e^{\beta_i \phi / M_{Pl}}. \tag{3.11}$$

While the first term $V(\phi)$ arises due to self-interactions, the second term comes from the conformal coupling to matter fields. It can also be observed that although $V(\phi)$ and $e^{\beta_i \phi / M_{Pl}}$ are monotonic functions, V_{eff} displays a minimum provided β_i is positive (see Figure (3.1)). If ϕ_{min} is the value assumed by ϕ at the minimum, it would satisfy

$$V_{,\phi}(\phi_{min}) + \sum_i \frac{\beta_i}{M_{Pl}} \rho_i e^{\beta_i \phi_{min} / M_{Pl}} = 0, \tag{3.12}$$

and the mass of small fluctuations around ϕ_{min} would be obtained as

$$m^2_{min} = \frac{d^2 V_{eff}}{d\phi^2} = V_{,\phi\phi}(\phi_{min}) + \sum_i \frac{\beta_i^2}{M_{Pl}^2} \rho_i e^{\beta_i \phi_{min} / M_{Pl}}. \tag{3.13}$$

Equations (3.12) and (3.13) show that the minimum value of the field ϕ_{min} and its mass m_{min} are both dependent on the local matter density ρ_i. It can also be observed that larger values of ρ_i imply a smaller ϕ_{min} and larger m_{min}. This means that the chameleon becomes more massive in denser environments. Therefore, this mechanism allows for the scalar field to be sufficiently massive on Earth to evade constraints on EP violations and fifth-force. The next chapter will discuss chameleon screening in the context of $f(R)$ gravity and its manifestation in the structure of non-linear mode-coupling kernels.

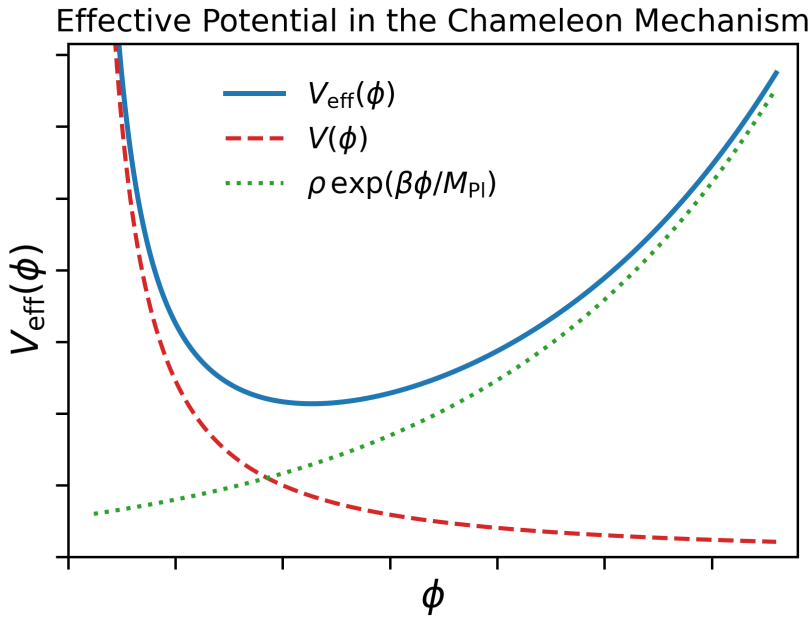

Figure 3.1: *Effective potential for the chameleon field as a sum of the self-potential $V(\phi)$ and the conformal coupling contribution $\rho e^{\beta\phi/M_{Pl}}$. These contributions produce a density-dependent minimum of the effective potential. In high-density regions, the minimum shifts to smaller values of ϕ and the curvature of V_{eff} increases, which implies a large effective mass for the scalar field. This represents the chameleon mechanism which screens the scalar-mediated 'fifth-force' in dense environments while allowing it to remain active on cosmological scales.*

Chapter 4

$f(R)$ Gravity and Screening

4.1 Introduction

$f(R)$ gravity is one of the simplest and most widely studied modifications to general relativity. It gained traction following Alexei Starobinsky's research on cosmic inflation [26], where a quadratic correction to the Ricci scalar R in the Einstein action produced a de Sitter universe that accounted for the accelerated expansion. Later on, it also emerged as a candidate to explain the late-time expansion of the universe, without invoking dark energy.

Through a conformal transformation, $f(R)$ theories can be recast as general relativity with an additional scalar degree of freedom that couples to all matter with a fixed coupling strength [11, 27]. This raises concerns over violations of the stringent solar system tests of gravity. However, screening mechanisms suppress the scalar degree of freedom in high-density environments, which effectively renders the theory indistinguishable from GR on such scales. As a result, $f(R)$ theories are not automatically ruled out. Further, it is possible to develop models that imitate a ΛCDM expansion history, but deviate from general relativity in the evolution of cosmological perturbations. In this chapter, we derive the quasi-static perturbation equations responsible for structure formation, and highlight how scale-dependent modifications to gravity enter the Poisson equation for $f(R)$ theories.

We consider theories of gravity that are governed by the following action,

$$S = \frac{1}{2\kappa^2}\int d^4x\sqrt{-g}[R + f(R)] + \int d^4x\sqrt{-g}\mathcal{L}_m[\chi_i, g_{\mu\nu}], \tag{4.1}$$

where $\kappa^2 = 8\pi G$ and $f(R)$ represents a general function of the Ricci scalar R. As the action is expressed in the Jordan frame, matter is minimally coupled to gravity and the matter fields χ_i follow the geodesics of the metric $g_{\mu\nu}$. Before proceeding, we adopt the notation $\partial f/\partial R \equiv f_R$ throughout this work. The field equation is obtained by varying the action with respect to the metric $g_{\mu\nu}$. We use the following components in the derivation:

- For a square matrix M, the following condition holds:

$$\begin{aligned} \delta(\det M) &= (\det M)\ \mathrm{Tr}\Big(M^{-1}\delta M\Big) \\ \therefore \quad \delta\sqrt{-g} &= \frac{1}{2}\sqrt{-g}\, g^{\mu\nu}\delta g_{\mu\nu} \end{aligned} \tag{4.2}$$

- The following identity holds:

$$\delta g_{\beta\nu} = -g_{\beta\mu}\cdot g_{\alpha\nu}\cdot \delta g^{\mu\alpha} \tag{4.3}$$

- It is also known that:

$$\delta\Gamma^{\rho}_{\mu\nu} = \frac{1}{2}g^{\rho\sigma}(\nabla_\mu\delta g_{\sigma\nu} + \nabla_\nu\delta g_{\sigma\mu} - \nabla_\sigma\delta g_{\mu\nu}) \tag{4.4}$$

  Substituting the identity from (4.3) in the above relation gives,

$$\begin{aligned} \delta\Gamma^{\rho}_{\mu\nu} &= -\frac{1}{2}g_{\alpha\nu}\nabla_\mu\delta g^{\rho\alpha} - \frac{1}{2}g_{\beta\mu}\nabla_\nu\delta g^{\rho\beta} + \frac{1}{2}g^{\rho\sigma}g_{\mu\alpha}g_{\nu\beta}\nabla_\sigma\delta g^{\alpha\beta} \\ \text{and} \quad \delta\Gamma^{\rho}_{\rho\mu} &= -\frac{1}{2}g_{\beta\rho}\nabla_\mu\delta g^{\rho\beta} \end{aligned} \tag{4.5}$$

- Lastly, the variation of the Ricci tensor $R_{\mu\nu}$ gives,

$$\delta R_{\mu\nu} = \nabla_\rho\delta\Gamma^{\rho}_{\nu\mu} - \nabla_\nu\delta\Gamma^{\rho}_{\rho\mu} \tag{4.6}$$

  Multiplying the equation by $g^{\mu\nu}$ and substituting the expressions from (4.5) gives,

$$g^{\mu\nu}\delta R_{\mu\nu} = -\nabla_\rho\nabla_\beta\delta g^{\rho\beta} + \Box(g_{\alpha\beta}\delta g^{\alpha\beta}) \tag{4.7}$$

But, it is known that $\delta R = R_{\mu\nu}\delta g^{\mu\nu} + g^{\mu\nu}\delta R_{\mu\nu}$. Therefore, it follows that,

$$\delta R = R_{\mu\nu}\delta g^{\mu\nu} + (g_{\mu\nu}\Box - \nabla_\mu\nabla_\nu)\delta g^{\mu\nu} \tag{4.8}$$

Before varying the action, it is convenient to decompose it into two parts as,

$$S = \underbrace{\frac{1}{2\kappa^2}\int d^4x\sqrt{-g}[R + f(R)]}_{S_g} + \underbrace{\int d^4x\sqrt{-g}\mathcal{L}_m[\chi_i, g_{\mu\nu}]}_{S_m} \tag{4.9}$$

- **Varying S_g:**

  The variation of the first part of the action, S_g, gives

$$\begin{aligned} \delta S_g &= \frac{1}{2\kappa^2}\int d^4x\big(\delta\sqrt{-g}(R+f) + \sqrt{-g}(\delta R + f_R\delta R)\big) \\ \therefore\quad \delta S_g &= \frac{1}{2\kappa^2}\int d^4x\sqrt{-g}\Bigg\{ -\frac{1}{2}g_{\mu\nu}(R+f(R))\delta g^{\mu\nu} \\ &\quad + (1+f_R)\Big[R_{\mu\nu}\delta g^{\mu\nu} + \big(\underbrace{g_{\mu\nu}\Box}_{\text{i}} - \underbrace{\nabla_\mu\nabla_\nu}_{\text{ii}}\big)\delta g^{\mu\nu}\Big]\Bigg\}. \end{aligned} \tag{4.10}$$

  The integral corresponding to the term $\mathcal{I}_i$ is evaluated,

$$\mathcal{I}_i = \frac{1}{2\kappa^2}\int d^4x\sqrt{-g}\{(1+f_R)g_{\mu\nu}\Box\delta g^{\mu\nu}\}. \tag{4.11}$$

  We assume that $(1+f_R)g_{\mu\nu} \equiv A_{\mu\nu}$. Using the covariant product rule,

$$A_{\mu\nu}\nabla_\alpha\nabla^\alpha\delta g^{\mu\nu} = \nabla_\alpha\left(A_{\mu\nu}\nabla^\alpha\delta g^{\mu\nu}\right) - \left(\nabla_\alpha A_{\mu\nu}\right)\nabla^\alpha\delta g^{\mu\nu}, \tag{4.12}$$

  the integral $\mathcal{I}_i$ becomes,

$$\begin{aligned} \mathcal{I}_i = &\frac{1}{2\kappa^2}\int d^4x\sqrt{-g}\nabla_\alpha(A_{\mu\nu}\nabla^\alpha\delta g^{\mu\nu}) \\ &-\frac{1}{2\kappa^2}\int d^4x\sqrt{-g}(\nabla_\alpha A_{\mu\nu})\nabla^\alpha\delta g^{\mu\nu}. \end{aligned} \tag{4.13}$$

  Since the first integrand in (4.13) is a total divergence, it reduces to a boundary term of the form,

$$\mathcal{I}_{i,a} = \frac{1}{2\kappa^2}\int_{\mathcal{M}} d^4x \partial_\alpha \left(\sqrt{-g} A_{\mu\nu}\nabla^\alpha \delta g^{\mu\nu}\right). \tag{4.14}$$

However, since we assume the variation of the metric to vanish at the boundary of the manifold, i.e., $\delta g_{\mu\nu}\big|_{\partial\mathcal{M}} = 0$, the integral $\mathcal{I}_{i,a}$ vanishes as well. Therefore, the integral $\mathcal{I}_i$ becomes

$$\mathcal{I}_i = -\frac{1}{2\kappa^2}\int d^4x\sqrt{-g}\nabla_\alpha[A_{\mu\nu}]\nabla^\alpha\delta g^{\mu\nu}. \tag{4.15}$$

Performing an integration by parts and discarding the boundary term once more, we arrive at

$$\begin{aligned} \mathcal{I}_i &= \frac{1}{2\kappa^2}\int d^4x\sqrt{-g}(\Box A_{\mu\nu})\delta g^{\mu\nu}, \\ \therefore \quad \mathcal{I}_i &= \frac{1}{2\kappa^2}\int d^4x\sqrt{-g}\, g_{\mu\nu}(\Box F(R))\delta g^{\mu\nu}. \end{aligned} \tag{4.16}$$

Similarly, the integral corresponding to the term $\mathcal{I}_{ii}$ is evaluated as

$$\mathcal{I}_{ii} = \frac{1}{2\kappa^2}\int d^4x\sqrt{-g}(1+f_R)(-\nabla_\mu\nabla_\nu)\delta g^{\mu\nu}. \tag{4.17}$$

Performing an integration by parts and neglecting the total divergence term, we obtain

$$\mathcal{I}_{ii} = \frac{1}{2}\int d^4x\sqrt{-g}\nabla_\mu(1+f_R)(\nabla_\nu\delta g^{\mu\nu}). \tag{4.18}$$

Repeating the integration by parts once again gives,

$$\mathcal{I}_{ii} = -\frac{1}{2\kappa^2}\int d^4x\sqrt{-g}\nabla_\mu\nabla_\nu f_R\delta g^{\mu\nu}. \tag{4.19}$$

Combining the two contributions from $\mathcal{I}_i$ and $\mathcal{I}_{ii}$, one obtains

$$\begin{aligned} \delta S_g = \frac{1}{2\kappa^2}\int d^4x\,\sqrt{-g}\Big\{&(1+f_R)R_{\mu\nu} - \frac{1}{2}g_{\mu\nu}\big(R+f(R)\big) \\ &+ \big(g_{\mu\nu}\Box - \nabla_\mu\nabla_\nu\big)f_R\Big\}\delta g^{\mu\nu}. \end{aligned} \tag{4.20}$$

- **Varying S_m:**

  Upon varying the matter sector of the action, we obtain

$$\delta S_m = \int d^4x \delta(\sqrt{-g}\,\mathcal{L}_m). \tag{4.21}$$

  Defining the stress-energy tensor as

$$T_{\mu\nu} = -\frac{2}{\sqrt{-g}}\frac{\delta(\sqrt{-g}\,\mathcal{L}_m)}{\delta g^{\mu\nu}}, \tag{4.22}$$

  the varied action becomes

$$\delta S_m = -\frac{1}{2}\int d^4x \sqrt{-g}\, T_{\mu\nu}\delta g^{\mu\nu}. \tag{4.23}$$

Combining the contributions from the two evaluated variations yields

$$\delta S = \delta S_g + \delta S_m = \frac{1}{2}\int d^4x\,\sqrt{-g}\left\{\frac{1}{\kappa^2}\Big[(1+f_R)R_{\mu\nu} - \frac{1}{2}g_{\mu\nu}(R+f(R)) + \big(g_{\mu\nu}\Box - \nabla_\mu\nabla_\nu\big)f_R\Big] - T_{\mu\nu}\right\}\delta g^{\mu\nu}. \tag{4.24}$$

However, the action must remain invariant under variations of the metric, yielding the field equations

$$\boxed{(1+f_R)R_{\mu\nu} - \frac{1}{2}g_{\mu\nu}\big(R+f(R)\big) + \big(g_{\mu\nu}\Box - \nabla_\mu\nabla_\nu\big)f_R = \kappa^2 T_{\mu\nu}} \tag{4.25}$$

The extra $f(R)$ term in the action leads to additional terms in the Einstein equations, which are now fourth-order differential equations.

The energy-momentum tensor of a perfect fluid can be expressed as

$$T_{\mu\nu} = (\rho + P)U_\mu U_\nu + P g_{\mu\nu}, \tag{4.26}$$

where ρ is the energy density, P is the pressure, and U^μ is the four-velocity in the rest frame. As the metric remains minimally coupled to

matter, the continuity equation is given as

$$\dot{\rho} + 3\mathcal{H}(\rho + P) = 0. \tag{4.27}$$

To derive the Friedmann equations, the FLRW metric is considered in conformal time,

$$ds^2 = a^2(\tau)[-d\tau^2 + \delta_{ij}dx^i dx^j]. \tag{4.28}$$

The following components are required in the derivation and are computed using the FLRW metric.

- **Christoffel symbols:** The non-zero Christoffel symbols are obtained as

$$\Gamma^0_{00} = \mathcal{H}, \qquad \Gamma^0_{ij} = \mathcal{H}\delta_{ij}, \qquad \Gamma^i_{0j} = \mathcal{H}\delta^i_j. \tag{4.29}$$

- **Ricci Tensor:** It is known that the Ricci tensor is defined as

$$R_{\mu\nu} = \partial_\sigma \Gamma^\sigma_{\mu\nu} - \partial_\nu \Gamma^\sigma_{\mu\sigma} + \Gamma^\sigma_{\sigma\rho}\Gamma^\rho_{\mu\nu} - \Gamma^\sigma_{\mu\rho}\Gamma^\rho_{\sigma\nu}. \tag{4.30}$$

  Using the Christoffel symbols, we can calculate:

$$R_{00} = -3\mathcal{H}', \qquad R_{ij} = \frac{\mathcal{H}' + 2\mathcal{H}^2}{a^2} g_{ij}. \tag{4.31}$$

- **Ricci Scalar:** The Ricci scalar is evaluated using

$$R = g^{\mu\nu} R_{\mu\nu}. \tag{4.32}$$

  Using the previous components, the Ricci scalar is obtained as

$$R = \frac{6(\mathcal{H}' + \mathcal{H}^2)}{a^2}. \tag{4.33}$$

- **4-Velocity and Stress-Energy Tensor:** The 4-velocity of a perfect fluid in a comoving frame is

$$U^\mu = \left(\frac{1}{a}, 0, 0, 0\right). \tag{4.34}$$

  Therefore, the 00 component of the stress–energy tensor takes the form

$$T_{00} = (\rho + P)U_\mu U_\nu + P g_{00} \Rightarrow T_{00} = \rho a^2. \tag{4.35}$$

The 00^{th} component of the Einstein equations gives

$$(1+f_R)R_{00} - \frac{1}{2}g_{00}(R+f) + (g_{00}\Box - \nabla_0\nabla_0)f_R = \kappa^2 T^{00}. \tag{4.36}$$

Upon using $\nabla_0 f_R = f_R'$, the equations reduce to

$$(1+f_R)(-3\mathcal{H}') - \frac{1}{2}(-a^2)\left[\frac{6(\mathcal{H}'+\mathcal{H}^2)}{a^2} + f\right] + 3\mathcal{H}f_R' = \kappa^2\rho a^2. \tag{4.37}$$

Further, noting that $\mathcal{H}' = a''/a - \mathcal{H}^2$, the first Friedmann equation is obtained as

$$\boxed{(1+f_R)\mathcal{H}^2 - \frac{a''}{a^2}f_R + \frac{a^2}{6}f + \mathcal{H}f_R' = \frac{\kappa^2}{3}a^2\rho} \tag{4.38}$$

From the ij^{th} component of the Einstein equations, one obtains

$$(1+f_R)R_{ij} - \frac{1}{2}g_{ij}(R+f) + (g_{ij}\Box - \nabla_i\nabla_j)f_R = \kappa^2 T_{ij}. \tag{4.39}$$

Using $\nabla_i\nabla_j f_R = -\mathcal{H}\delta_{ij}f_R'$ and $T_{ij} = Pa^2\delta_{ij}$, along with the results from equations (4.31) and (4.33) one finds

$$(1+f_R)\left(\frac{a''}{a} + \mathcal{H}^2\right) - 3\left(\frac{a''}{a}\right) - \frac{a^2}{2}f - f_R'' - \mathcal{H}f_R' = \kappa^2 a^2 P. \tag{4.40}$$

Subtracting equation (4.38) from the above expression gives

$$\frac{a''}{a}(1-f_R) + \frac{a^2}{3}f + \frac{f_R''}{2} + \mathcal{H}f_R' = -\frac{\kappa^2 a^2}{6}(3P-\rho). \tag{4.41}$$

However, from equation (4.38), it is known that

$$\mathcal{H}f_R' = \frac{\kappa^2}{3}a^2\rho - (1+f_R)\mathcal{H}^2 + \frac{a''}{a}f_R - \frac{a^2}{6}f \tag{4.42}$$

Upon substitution into equation (4.41), the second Friedmann equation

is obtained as

$$\boxed{\frac{a''}{a} + \frac{a^2}{6}f + \frac{f_R''}{2} - (1+f_R)\mathcal{H}^2 = -\frac{\kappa^2}{6}a^2(3P+\rho)} \tag{4.43}$$

The additional terms that arise in the Friedmann equations due to $f(R) \neq 0$ effectively replace dark energy [11]. In particular, this new scalar degree of freedom is denoted by f_R, and is called the *scalaron* [26].

Taking the trace of the Einstein field equation (4.25) gives

$$\Box f_R = \frac{1}{3}(R + 2f - Rf_R) - \frac{\kappa^2}{3}(\rho - 3P) = \frac{\partial V_{\text{eff}}}{\partial f_R} \tag{4.44}$$

Therefore, a second-order equation for the field f_R is obtained, with a canonical kinetic term and an effective potential sourced by the scalaron. To remain consistent with the theoretical predictions of the early universe, when curvature was large, the following assumptions must hold [11]:

$$|f| \ll R, \qquad |f_R| \ll 1. \tag{4.45}$$

This ensures the restoration of the theory to general relativity in the high curvature limit.

The extremum of the effective potential V_{eff} is given by setting

$$\frac{dV_{\text{eff}}}{df_R} = \frac{1}{3}(R + 2f - Rf_R) - \frac{\kappa^2}{3}(\rho - 3P) = 0, \tag{4.46}$$

which in the high curvature limit reduces to its GR value

$$R = \frac{\kappa^2}{3}(\rho - 3P). \tag{4.47}$$

Furthermore, the mass of the scalaron is determined by the second derivative of the effective potential,

$$m_{f_R}^2 = \frac{\partial^2 V_{\text{eff}}}{\partial f_R^2} = \frac{1}{3}\left[\frac{1+f_R}{f_{RR}} - R\right]. \tag{4.48}$$

In the high curvature limit, the mass can be approximated as

$$m_{f_R}^2 \approx \frac{1+f_R}{f_{RR}} \approx \frac{1}{3f_{RR}}. \tag{4.49}$$

This implies that the condition $f_{RR} > 0$ must be satisfied in order to avoid a tachyonic scalaron. Furthermore, the mass of the scalaron m_{f_R} sets the Compton wavelength

$$\lambda_C = \frac{2\pi}{m_{f_R}}. \tag{4.50}$$

The range of the fifth-force mediated by the scalaron is determined by its Compton wavelength. Therefore, in regions of high density, where the scalaron becomes heavier, the range of the fifth force is significantly reduced and its effects become unobservable. This is the manifestation of chameleon screening in the context of $f(R)$ gravity.

4.1.1 Viable $f(R)$ Gravity Models

The viability of $f(R)$ models is constrained by stringent observational and experimental bounds. While $f(R)$ gravity is formally equivalent to Brans-Dicke theory with $\omega_{\text{BD}} = 0$, low values of the parameter are ruled out by solar system tests. However, in high-density regimes, the scalar degree of freedom becomes heavier and therefore strongly suppressed. This necessitates a separate set of conditions that the theory must satisfy to remain observationally consistent.

The conditions that $f(R)$ gravity models must satisfy to be a viable theory which explains cosmic acceleration are as follows [11]:

1. For $R \gg f_{RR}$, $f_{RR} > 0$. As implied by equation (4.49), a positive f_{RR} ensures that the scalaron does not experience tachyonic instabilities. Classically, this condition arises from requiring a stable high-curvature regime, such as the matter-dominated epoch [28].

2. $1 + f_R$ at all finite R. Since the effective Newton constant in case of $f(R)$ gravity is given by

$$G_{\text{eff}} = \frac{G}{1+f_R}, \tag{4.51}$$

this condition ensures that the sign of the gravitational constant does not change. Quantum mechanically, it prevents the graviton from becoming a ghost [29], while classically, $1 + f_R < 0$ implies a universe that quickly becomes inhomogeneous and anisotropic [30, 31].

3. Since CMB and Big Bang nucleosynthesis observations require GR to be recovered at earlier times, this means $f(R)/R \to 0$ and $f_R \to 0$ as $R \to \infty$. However, since $f_{RR} > 0$, this implies that $f_R < 0$ for all R, with f_R being a monotonically increasing function that tends to zero asymptotically.

We use these conditions repeatedly across the thesis to ensure the agreement of theory with observations.

4.2 Perturbations in $f(R)$ Models

Perturbations around the Friedmann–Lemaître–Robertson–Walker metric are expressed in the Newtonian gauge, which is given as follows:

$$ds^2 = -(1+2\psi)dt^2 + a^2(1+2\phi)\delta_{ij}dx^i dx^j. \tag{4.52}$$

The evolution of matter fluctuations is studied within the Hubble horizon. Before proceeding, it is important to discuss the quasi-static approximation and its role in deriving the equations governing the growth of cosmological perturbations. In theories of modified gravity/dark energy, it is based on the assumption that relevant modes satisfy $k \gg aH$, such that the spatial derivatives dominate over the time derivatives. This implies $\ddot{\phi} \ll c_s^2 k^2 \delta\phi$. Physically, this means that the perturbations evolve slowly compared to the timescale set by their spatial propagation. This allows the scalar fields to adjust instantaneously to changes in the matter density, and can effectively be treated as remaining in equilibrium with the matter distribution.

As discussed earlier, in order to successfully explain the accelerated expansion of the universe, gravity must be modified on large scales. However, such modifications introduce scalar degrees of freedom that alter dynamics even on sub-horizon scales. These modifications can be described using Brans-Dicke gravity. In this context, $f(R)$ gravity can be considered as a scalar-tensor theory equivalent to a Brans-Dicke model with the parameter $\omega_{\rm BD} = 0$ and a specific scalar potential. Therefore, using the

quasi-static approximation, the perturbed modified Einstein equations are given as [32],

$$\phi + \psi = -\varphi \tag{4.53}$$

$$\frac{1}{a^2}\nabla^2\psi = 4\pi G\rho_m\delta - \frac{1}{2a^2}\nabla^2\varphi. \tag{4.54}$$

Here, φ is the scalar field perturbation associated with the additional scalar degree of freedom in scalar-tensor theories. Furthermore, equation (4.53) encodes the gravitational slip that is induced due to the departure from general relativity.

The equation of motion for the scalar field perturbation is given by [32],

$$(3 + 2\omega_{BD})\frac{1}{a^2}\nabla^2\varphi = -8\pi G\rho_m\delta, \tag{4.55}$$

where ρ_m is the background energy density and δ is the density contrast of dark matter.

Many modified gravity models that address the late-time cosmic acceleration predict a Brans-Dicke parameter $\omega_{\rm BD}$ of order unity on sub-horizon scales. Such values do not agree with the stringent Solar System constraints, which require $\omega_{\rm BD} > 40000$ [8]. However, these bounds only apply if the scalar has no potential or self-interactions. When an interaction term is introduced, the scalar field becomes effectively screened in dense regions, thereby evading local constraints. In this case, the dynamics of the scalar perturbation obeys a field equation of the form

$$\frac{3}{a^2}k^2\varphi = 8\pi G\rho_m\delta - \mathcal{I}(\varphi), \tag{4.56}$$

where the interaction term $\mathcal{I}$ can be expanded as [32],

$$\begin{aligned}\mathcal{I}(\varphi) = M_1(k)\varphi + \frac{1}{2}\int \frac{d^3\mathbf{k}_1 d^3\mathbf{k}_2}{(2\pi)^3}\delta_D(\mathbf{k}-\mathbf{k}_{12})M_2(\mathbf{k}_1,\mathbf{k}_2)\varphi(\mathbf{k}_1)\varphi(\mathbf{k}_2)\\ +\frac{1}{6}\int \frac{d^3\mathbf{k}_1 d^3\mathbf{k}_2 d^3\mathbf{k}_3}{(2\pi)^6}\delta_D(\mathbf{k}-\mathbf{k}_{123})M_3(\mathbf{k}_1,\mathbf{k}_2,\mathbf{k}_3)\varphi(\mathbf{k}_1)\varphi(\mathbf{k}_2)\varphi(\mathbf{k}_3).\end{aligned} \tag{4.57}$$

One realisation of this non-linear interaction term $\mathcal{I}$ is provided by the

chameleon mechanism, which has been discussed in Chapter 3. With an increase in local mass density, the scalar field becomes heavier, thereby suppressing departures from general relativity. In the above expression, M_1 is the linear mass term of the scalar perturbation in the background, while M_i ($i > 1$) represent the higher-order self-interaction coefficients that describe how the mass changes with energy density [32].

The next step is to derive the complete form of the modified, perturbed Poisson equation. To this end, the interaction term can be substituted within equation (4.56) giving,

$$\frac{3}{a^2}k^2\varphi(\mathbf{k}) + M_1\varphi(\mathbf{k}) = \kappa^2\rho_m\delta(\mathbf{k}) - \mathcal{I}_{NL}(\mathbf{k}), \tag{4.58}$$

where $\mathcal{I}_{NL}$ includes all the higher-order non-linear contributions to the interaction term $\mathcal{I}$. For ease of notation, it is also convenient to define,

$$\Pi(\mathbf{k}) = \frac{k^2}{a^2} + \frac{M_1}{3}. \tag{4.59}$$

Therefore, $\varphi(\mathbf{k})$ in equation (4.58) can be re-expressed as,

$$\varphi(\mathbf{k}) = \frac{1}{3\Pi(\mathbf{k})}\left[\kappa^2\rho_m\delta(\mathbf{k}) - \mathcal{I}_{NL}\right]. \tag{4.60}$$

We can perturbatively expand φ as,

$$\varphi = \varphi^{(1)} + \varphi^{(2)} + \varphi^{(3)} + ... \tag{4.61}$$

Upon comparing equations (4.60) and (4.61), it is straightforward to see that the linear contribution is given by,

$$\varphi^{(1)} = \frac{\kappa^2\rho_m\delta(\mathbf{k})}{3\Pi(\mathbf{k})}. \tag{4.62}$$

Similarly, the quadratic contribution is obtained from the first term of $\mathcal{I}_{NL}$ which reads,

$$\mathcal{I}^{(2)}_{NL}(\mathbf{k}) = \frac{1}{2}\int \frac{d^3\mathbf{k}_1 d^3\mathbf{k}_2}{(2\pi)^3}\delta_D(\mathbf{k}-\mathbf{k}_{12})M_2(\mathbf{k}_1,\mathbf{k}_2)\varphi^{(1)}(\mathbf{k}_1)\varphi^{(1)}(\mathbf{k}_2). \tag{4.63}$$

Substituting the expression for $\varphi^{(1)}$ from equation (4.62) yields,

$$\mathcal{I}^{(2)}_{NL}(\mathbf{k}) = -\frac{(\kappa^2\rho_m)^2}{6\Pi(\mathbf{k})}\int \frac{d^3\mathbf{k}_1 d^3\mathbf{k}_2}{(2\pi)^3}\delta_D(\mathbf{k}-\mathbf{k}_{12})M_2(\mathbf{k}_1,\mathbf{k}_2)\frac{\delta(\mathbf{k}_1)\delta(\mathbf{k}_2)}{\Pi(\mathbf{k}_1)\Pi(\mathbf{k}_2)}. \tag{4.64}$$

However, it follows from equations (4.60) and (4.61) that,

$$\varphi^{(2)}(\mathbf{k}) = -\frac{I^{(2)}_{NL}(\mathbf{k})}{3\Pi(\mathbf{k})}. \tag{4.65}$$

Therefore, we obtain,

$$\varphi^{(2)}(\mathbf{k}) = -\frac{(\kappa^2\rho_m)^2}{3^2\times 6\Pi(\mathbf{k})}\int \frac{d^3\mathbf{k}_1 d^3\mathbf{k}_2}{(2\pi)^3}\delta_D(\mathbf{k}-\mathbf{k}_{12})M_2(\mathbf{k}_1,\mathbf{k}_2)\frac{\delta(\mathbf{k}_1)\delta(\mathbf{k}_2)}{\Pi(\mathbf{k}_1)\Pi(\mathbf{k}_2)}. \tag{4.66}$$

Similarly, the cubic-order contribution receives two terms: one arising from the product of three first-order perturbations $\varphi^{(1)}$ and another from the product of one first and one second-order perturbations ($\varphi^{(1)}$ and $\varphi^{(2)}$). Therefore, one obtains,

$$\begin{aligned}\varphi^{(3)}(\mathbf{k}) = -\frac{1}{18\Pi(\mathbf{k})}\left(\frac{\kappa^2\rho_m}{3}\right)^3 \int \frac{d^3\mathbf{k}_1 d^3\mathbf{k}_2 d^3\mathbf{k}_3}{(2\pi)^6}\delta_D(\mathbf{k}-\mathbf{k}_{123}) \\ \times\left\{M_3(\mathbf{k}_1,\mathbf{k}_2,\mathbf{k}_3) - \frac{M_2(\mathbf{k}_1,\mathbf{k}_2+\mathbf{k}_3)M_2(\mathbf{k}_2,\mathbf{k}_3)}{\Pi(\mathbf{k}_{23})}\right\} \\ \times\frac{\delta(\mathbf{k}_1)\delta(\mathbf{k}_2)\delta(\mathbf{k}_3)}{\Pi(\mathbf{k}_1)\Pi(\mathbf{k}_2)\Pi(\mathbf{k}_3)}.\end{aligned} \tag{4.67}$$

Moving forward, we adopt the following notation for convenience,

$$S(\mathbf{k}) = \varphi^{(2)} + \varphi^{(3)} + ... \tag{4.68}$$

where $S(\mathbf{k})$ represents the non-linear source term of perturbations. To obtain the full form of the Poisson equation, equation (4.60) is substituted in the Poisson equation (4.54). Moving to Fourier space gives

$$-\frac{k^2}{a^2}\psi(\mathbf{k}) = \frac{\kappa^2\rho_m\delta(\mathbf{k})}{2}\left[1+\frac{k^2/a^2}{3\Pi(\mathbf{k})}\right] - \frac{1}{2}\frac{k^2}{a^2}\frac{\mathcal{I}_{NL}(\mathbf{k})}{3\Pi(\mathbf{k})}, \tag{4.69}$$

where $\kappa^2 = 8\pi G$. Therefore, the Poisson equation is obtained as,

$$\boxed{-\left(\frac{k}{a}\right)^2\psi(\mathbf{k}) = \frac{1}{2}\kappa^2\rho_m\left[1+\frac{1}{3}\frac{(k/a)^2}{\Pi(\mathbf{k})}\right] + \frac{1}{2}\left(\frac{k}{a}\right)^2 S(\mathbf{k}),} \tag{4.70}$$

where the non-linear source term, up to third-order, is given by

$$\begin{aligned} S(\mathbf{k}) = &-\frac{1}{6\Pi(\mathbf{k})}\left(\frac{\kappa^2\rho_m}{3}\right)^2\int\frac{d^3\mathbf{k}_1 d^3\mathbf{k}_2}{(2\pi)^3}\delta_D(\mathbf{k}-\mathbf{k}_{12})M_2(\mathbf{k}_1,\mathbf{k}_2)\frac{\delta(\mathbf{k}_1)\delta(\mathbf{k}_2)}{\Pi(\mathbf{k}_1)\Pi(\mathbf{k}_2)} \\ &-\frac{1}{18\Pi(\mathbf{k})}\left(\frac{\kappa^2\rho_m}{3}\right)^3\int\frac{d^3\mathbf{k}_1 d^3\mathbf{k}_2 d^3\mathbf{k}_3}{(2\pi)^6}\delta_D(\mathbf{k}-\mathbf{k}_{123})\Bigg\{M_3(\mathbf{k}_1,\mathbf{k}_2,\mathbf{k}_3) \\ &-\frac{M_2(\mathbf{k}_1,\mathbf{k}_{23})M_2(\mathbf{k}_2,\mathbf{k}_3)}{\Pi(\mathbf{k}_{23})}\Bigg\}\frac{\delta(\mathbf{k}_1)\delta(\mathbf{k}_2)\delta(\mathbf{k}_3)}{\Pi(\mathbf{k}_1)\Pi(\mathbf{k}_2)\Pi(\mathbf{k}_3)}. \end{aligned} \tag{4.71}$$

The forms of M_1, M_2, M_3, and Π depend on the specific model of modified gravity under consideration. In the next chapter, these functions will be specified explicitly for the class of models being studied. We will also examine how these functions enter the higher-order statistics governing non-linear structure formation.

Chapter 5

Interaction Coefficients of Hu-Sawicki $f(R)$ Gravity

This chapter specialises the quasi-non-linear perturbative framework to $f(R)$ gravity. The main aim is to derive the ingredients required to compute the matter power spectrum, specifically the interaction coefficients M_1, M_2, M_3, and the function Π. This also makes it possible to examine how these functions encode the scale dependence and screening behavior characteristic of $f(R)$ theories.

As extensively discussed earlier, $f(R)$ theories are governed by the action,

$$S = \int d^4x\sqrt{-g}\left[\frac{R + f(R)}{2\kappa^2} + \mathcal{L}_m\right]. \tag{5.1}$$

The trace of the field equations associated with this action has also been derived as

$$3\Box f_R - R + f_R \cdot R - 2f(R) = -\kappa^2\rho_m, \tag{5.2}$$

where ρ_m is the matter density of dark matter and $\kappa^2 = 8\pi G$. In $f(R)$ gravity, the additional scalar degree of freedom is f_R and its field perturbation is given by

$$\varphi = \delta f_R = f_R - \bar{f_R}, \tag{5.3}$$

where $\bar{f_R}$ represents the value of the scalar field in the background. The perturbations around the Ricci scalar and matter density are defined as

$$R = \bar{R} + \delta R \tag{5.4}$$

$$\rho = \bar{\rho}(1+\delta). \tag{5.5}$$

Perturbing the field equations (5.2) gives

$$\begin{aligned} 3\Box(\bar{f_R}+\varphi) - (\bar{R}+\delta R) + (\bar{f_R}+\varphi)(\bar{R}+\delta R) \\ -2(\bar{f}+\delta f) = -\kappa^2(\bar{\rho}_m + \bar{\rho}_m\delta_m). \end{aligned} \tag{5.6}$$

The background field equation is subtracted from the above expression to obtain

$$3\Box\varphi - \delta R + \bar{f_R}\delta R + \varphi\bar{R} - 2\delta f = -\kappa^2\bar{\rho}_m\delta_m. \tag{5.7}$$

Applying the quasi-static approximation, in which time derivatives are neglected relative to spatial derivatives, reduces the expression to

$$-\frac{3}{a^2}\nabla^2\varphi - \delta R(1-\bar{f_R}) - 2\delta f = -\kappa^2\bar{\rho}_m\delta_m. \tag{5.8}$$

The change in $f(R)$ can be obtained by performing a Taylor expansion up to first order as

$$f(R) = \bar{f}(R) + \left.\frac{\partial f}{\partial R}\right|_{R=\bar{R}}(R-\bar{R}) \tag{5.9}$$

$$\therefore \delta f = \bar{f_R}\delta R. \tag{5.10}$$

Furthermore, to ensure that the background expansion closely resembles that of ΛCDM cosmology, the following approximations are applied [32],

$$|\bar{f_R}| \ll 1, \quad |\bar{f}/\bar{R}| \ll 1. \tag{5.11}$$

Applying these approximations to equation (5.8) yields

$$-\frac{3}{a}\nabla^2\varphi - \delta R = -\kappa^2\rho_m\delta_m. \tag{5.12}$$

In the next step, this equation of motion for the scalar field perturbation is compared against the general scalar equation (4.56) introduced in the previous chapter. This comparison allows for the identification of the interaction term in the case of $f(R)$ theories, which we obtain as

$$\mathcal{I}(\varphi) = \delta R = R(f_R) - R(\bar{f_R}). \tag{5.13}$$

Performing a Taylor expansion about the background value once again gives the perturbative expansion of the interaction term up to third order,

$$\mathcal{I}(\varphi) = \delta R = \left.\frac{\partial R(f_R)}{\partial f_R}\right|_{f_R=\bar{f}_R} \varphi + \frac{1}{2}\cdot\left.\frac{\partial^2 R(f_R)}{\partial f_R^2}\right|_{f_R=\bar{f}_R} \varphi^2 + \frac{1}{6}\cdot\left.\frac{\partial^3 R(f_R)}{\partial f_R^3}\right|_{f_R=\bar{f}_R} \varphi^3. \tag{5.14}$$

Comparing this to the general expansion of the interaction term from the previous Chapter, equation (4.57), allows us to observe that,

$$\boxed{M_1 = \left.\frac{\partial R(f_R)}{\partial f_R}\right|_{f_R=\bar{f}_R}, \quad M_2 = \left.\frac{\partial^2 R(f_R)}{\partial f_R^2}\right|_{f_R=\bar{f}_R}, \quad M_3 = \left.\frac{\partial^3 R(f_R)}{\partial f_R^3}\right|_{f_R=\bar{f}_R}.} \tag{5.15}$$

The explicit forms of M_1, M_2, and M_3 are model-dependent and in the next section, these quantities will be derived for the Hu-Sawicki model of $f(R)$ gravity.

5.1 Hu-Sawicki Model

In 2007, Wayne Hu and Ignacy Sawicki proposed a class of $f(R)$ models that could reproduce an expansion history similar to that of the ΛCDM universe without invoking the cosmological constant [33]. These are among a limited set of functional $f(R)$ constructions that satisfy the solar system tests of gravity.

The Hu-Sawicki model with chameleon screening takes the form [33],

$$f(R) = -m^2 \frac{c_1 (R/m^2)^n}{c_2 (R/m^2)^n + 1}, \tag{5.16}$$

and when $n = 1$, it gives

$$f(R) \propto \frac{R}{AR + 1}, \tag{5.17}$$

for some constant A. In the high curvature regime, when $AR \gg 1$, $f(R)$ can be expanded as

$$f(R) \simeq -2\kappa^2\rho_\Lambda - f_{R0}\frac{R_0^2}{R}, \tag{5.18}$$

where f_{R0} is the free parameter of the theory. Therefore, the first derivative of $f(R)$ with respect to the curvature R is given by,

$$f_R = f_{R0}\frac{R_0^2}{R^2} \Rightarrow R = \sqrt{\frac{f_{R0}R_0^2}{f_R}}, \tag{5.19}$$

and assuming a ΛCDM background,

$$R_0 = H_0^2(12 - 9\Omega_{m0}). \tag{5.20}$$

Introducing a dimensionless variable [34],

$$E \equiv \frac{H^2}{H_0^2}, \tag{5.21}$$

where, assuming a ΛCDM background, one obtains

$$E = \Omega_m a^{-3} + (1 - \Omega_m). \tag{5.22}$$

The background functions that appear in the Friedmann equations can be expressed in terms of E and E' [11],

$$\frac{R}{H_0^2} = 3(4E + E'), \tag{5.23}$$

where a prime denotes differentiation with respect to $\ln a$. Therefore, for the assumed ΛCDM background, one obtains an expression for the Ricci scalar R as

$$R = 3H_0^2(\Omega_{m0}a^{-3} + 4(1 - \Omega_{m0})). \tag{5.24}$$

However, using equations (5.15) and (5.19), the expression for M_1 in the Hu-Sawicki model can be found as

$$M_1 = -\frac{R^3}{2}\frac{1}{f_{R0}R_0^2}\bigg|_{f_R=\bar{f}_R}. \tag{5.25}$$

Substituting the background expression for the Ricci scalar from equation (5.24) yields,

$$\boxed{M_1 = -\frac{1}{2|f_{R0}|}\,\frac{3H_0^2\left(\Omega_{m0} - 4a^3(\Omega_{m0}-1)\right)^3}{a^9\left(4-3\Omega_{m0}\right)^2}.} \tag{5.26}$$

Consequently, the expression for $\Pi(\mathbf{k})$ follows directly from equation (4.59) as

$$\boxed{\Pi(\mathbf{k},a) = \frac{k^2}{a^2} + \frac{1}{2|f_{R0}|}\,\frac{H_0^2\left(\Omega_{m0} - 4a^3(\Omega_{m0}-1)\right)^3}{a^9\left(4-3\Omega_{m0}\right)^2}} \tag{5.27}$$

Similarly, the expression for M_2 in the Hu-Sawicki model is given by

$$M_2 = \frac{3}{4}\frac{R^5}{(f_{R0}R_0)^2}. \tag{5.28}$$

Substituting the expressions from equations (5.20) and (5.24) gives,

$$\boxed{M_2 = \frac{9}{4}\frac{H_0^2\left(\Omega_{m0} + 4(1-\Omega_{m0})a^3\right)^5}{|f_{R0}|^2 a^{15}\left(4-3\Omega_{m0}\right)^4}.} \tag{5.29}$$

Lastly, the expression for M_3 in the Hu-Sawicki model is,

$$M_3 = -\frac{15}{8}\frac{R^7}{(f_{R0}R_0^2)^3}. \tag{5.30}$$

Substituting the expressions from equations (5.20) and (5.24) gives,

$$\boxed{M_3 = -\frac{45}{8}\,\frac{H_0^2\left(\Omega_{m0} + 4a^3(1-\Omega_{m0})\right)^7}{a^{21}\left|f_{R0}\right|^3\left(4-3\Omega_{m0}\right)^4}.} \tag{5.31}$$

This completes the derivation of the interaction coefficients that encode the screening mechanism relevant to the theory. With the interaction coefficients now completely specified, the Poisson equation determines how the gravitational potential ψ responds to matter density perturbations and screening. This potential acts as a source term in the Euler equation (2.10) which determines the evolution of the peculiar velocity field. Combined with the continuity equation, it forms a closed system that determines the evolution of matter perturbations. As seen in Chapter 2, this system is solved by assuming a perturbative Ansatz created from the convolution of linear density fields and the mode coupling kernels F_n and G_n. These kernels enter the non-linear matter power and imprint signatures of screening and scale-dependent growth.

Chapter 6

Numerical Analysis of Modified Poisson Equation Vertices

In the previous chapter, the exact form of the modified Poisson equation in the case of the Hu-Sawicki model of $f(R)$ gravity was derived. This chapter presents a numerical analysis that explicitly computes the linear and non-linear vertices appearing in the Poisson equation, and studies their scale and time dependence. Plotting these vertices helps identify regimes in which deviations from general relativity become significant, as well as regions where screening suppresses the effects of modified gravity.

This analysis depends on the background cosmology, the Hu-Sawicki model parameter f_{R0}, and the theoretical assumptions used in the previous chapters. The model is constructed assuming a flat ΛCDM background, specified by the Hubble constant $H_0 = 67.9\,\mathrm{km/s/Mpc}$ and the matter density parameter $\Omega_m = 0.303$ which were adopted from the 2018 Planck cosmological analysis [35].

The modified gravity contributions are characterised by the parameter f_{R0}, which controls the overall strength of deviation from general relativity. It enters both the linear and non-linear vertices that appear in the modified Poisson equation. It also sets the Compton wavelength below which modifications to gravity become relevant and above which they are screened. The different assumption adopted in the previous chapters are retained during this analysis. This includes the subhoriozon quasi-static approximation and the assumptions required to ensure viable $f(R)$ theories.

The main aim of this numerical implementation is to evaluate the ver-

tices over scale and time, and determine where their respective contributions are dominant. We perform the computation using the scale factor a as the time variable and the vertices are studied over the range $a \in [10^{-3}, 1]$, effectively covering the entire history of cosmic evolution while maintaining numerical stability. The scale dependence is sampled over the range $k \in [10^{-3}, 1.2]\, h\, Mpc^{-1}$, which spans the linear and quasi-non-linear regimes of structure formation. A uniform grid of scale and time is constructed in these ranges, over which the vertices are studied.

During this analysis, an alternate convention is adopted for ease of notation [36]. The modified Poisson equation reads,

$$\begin{aligned}
-\frac{k^2}{\mathcal{H}^2}\,\Psi(\mathbf{k},a) = {} & \frac{3\Omega_m}{2}\,\nu(a,k)\,\delta_{\mathbf{k}}(a) \\
& + \left(\frac{3\Omega_m}{2}\right)^2 \int_{\mathbf{k}_1,\mathbf{k}_2} (2\pi)^3 \delta_D(\mathbf{k}-\mathbf{k}_{12})\,\nu_2(a,k)\,\delta_{\mathbf{k}_1}(a)\,\delta_{\mathbf{k}_2}(a) \\
& + \left(\frac{3\Omega_m}{2}\right)^3 \int_{\mathbf{k}_1,\mathbf{k}_2,\mathbf{k}_3} (2\pi)^3 \delta_D(\mathbf{k}-\mathbf{k}_{123})\,\nu_3(a,k)\,\delta_{\mathbf{k}_1}(a)\,\delta_{\mathbf{k}_2}(a)\,\delta_{\mathbf{k}_3}(a) \\
& + \left(\frac{3\Omega_m}{2}\right)^3 \int_{\mathbf{k}_1,\mathbf{k}_2,\mathbf{k}_3} (2\pi)^3 \delta_D(\mathbf{k}-\mathbf{k}_{123})\,\nu_{22}(a,k)\,\delta_{\mathbf{k}_1}(a)\,\delta_{\mathbf{k}_2}(a)\,\delta_{\mathbf{k}_3}(a)\,,
\end{aligned} \tag{6.1}$$

where ν is the linear vertex and ν_2, ν_3, and ν_{22} are the non-linear vertices. Using $\Omega_m = \kappa^2\rho_m/3H(a)^2$ and comparing with equations (4.70) and (4.71), we obtain

$$\nu(a,k) = 1 + \frac{1}{3}\frac{(k/a)^2}{\Pi(\mathbf{k})} \tag{6.2}$$

$$\nu_2(a,k) = -\left(\frac{k}{a}\right)^2 \frac{H(a)^2}{128}\frac{M_2(\mathbf{k}_1,\mathbf{k}_2)}{\Pi(\mathbf{k})\Pi(\mathbf{k}_1)\Pi(\mathbf{k}_2)} \tag{6.3}$$

$$\nu_3(a,k) = -\frac{2H(a)^4}{243}\left(\frac{k}{a}\right)^2 \frac{M_3(\mathbf{k}_1,\mathbf{k}_2,\mathbf{k}_3)}{\Pi(\mathbf{k})\Pi(\mathbf{k}_1)\Pi(\mathbf{k}_2)\Pi(\mathbf{k}_3)} \tag{6.4}$$

$$\nu_{22}(a,k) = \frac{2H(a)^4}{243}\left(\frac{k}{a}\right)^2 \frac{M_2(\mathbf{k}_1,\mathbf{k}_{23})M_2(\mathbf{k}_2,\mathbf{k}_3)}{\Pi(\mathbf{k})\Pi(\mathbf{k}_1)\Pi(\mathbf{k}_2)\Pi(\mathbf{k}_3)\Pi(\mathbf{k}_{23})}, \tag{6.5}$$

where M_1, M_2, and M_3 are model-dependent and, in this case, specified by equations (5.25), (5.28), and (5.30).

In addition to the evolution of the Poisson equation vertices, the Compton scale associated with the scalar degree of freedom is also plotted in all figures. As seen in equation (6.7), the Compton wavelength is determined by the scalaron mass and sets the characteristic scale which separates the screened and unscreened regimes.

It is plotted in the (a, k) plane using the time-dependent scalaron mass of the Hu-Sawicki model. The comoving Compton scale is given by:

$$k_C(a) = \frac{a m_{f_R(a)}}{2\pi}, \tag{6.6}$$

where

$$m_{f_R} \equiv \sqrt{\frac{\bar{R}_f}{3}} = \left(\frac{R_0}{6|\bar{f}_R|} \sqrt{\frac{f_{R0}}{\bar{f}_R}} \right)^{\frac{1}{2}}. \tag{6.7}$$

The Compton crossing is evaluated numerically and overlaid on the vertex plots as a white dashed curve. This curve serves as a visual marker separating the regions where the fifth force is screened and where modified gravity effects are active.

6.1 Scale and Time Dependence of the Vertices

6.1.1 Linear Vertex and the Low Curvature Regime

The vertex ν incorporates the scale-dependent modifications to the gravitational coupling at linear order. In Figure (6.1), ν is evaluated over the (a, k) plane for the Hu-Sawicki model, for two different values of the parameter: $f_{R0} = -10^{-6}$ and $f_{R0} = -10^{-4}$. The dashed curve indicates the Compton crossing $k/a \sim m(a)$, which represents the transition between the regimes where the scalar field is light and mediates a long-range force, and where it is heavy and screening sets in.

We know that the linear vertex encodes the scale-dependent modifications to gravity through the expression

$$\nu(a, k) = 1 + \frac{1}{3} \frac{(k/a)^2}{\Pi(\mathbf{k})} \tag{6.8}$$

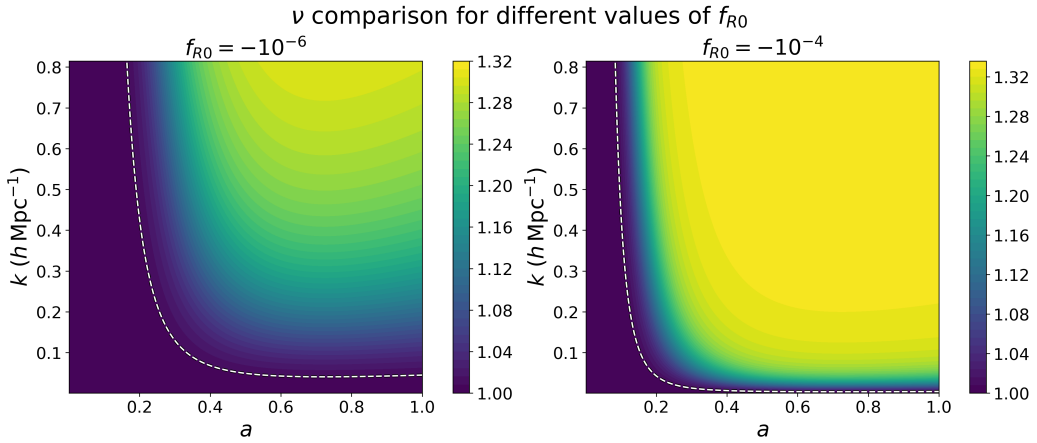

Figure 6.1: *Scale and time dependence of the linear vertex $\nu(a,k)$ for two values of the Hu-Sawicki $f(R)$ parameter: $|f_{R0}| = 10^{-6}$ (left panel) and $|f_{R0}| = 10^{-4}$ (right panel). The dashed curve represents the Compton crossing, separating the screened (high-curvature) and unscreened (low-curvature) regimes.*

and that it controls the response of the gravitational potential to linear matter perturbations. From Figure (6.1), one can observe that at early times, across all scales, $\nu \simeq 1$, which represents the recovery of general relativity. This agrees with the theoretical prediction that the modifications are exponentially suppressed at high curvatures, since the scalaron acquires a large mass (i.e., short-range). It also satisfies the viability condition that $f(R)$ cosmology must mimic ΛCDM in the high-redshift regime where it is well-tested and constrained by cosmic microwave background observations [33, 37, 38].

Furthermore, using equations (6.7) and (6.8), we can express the linear vertex as

$$\nu(a,k) = 1 + \frac{1}{3}\frac{(k/a)^2}{(k/a)^2 + m^2(a)}. \tag{6.9}$$

In the deep-Compton limit, $(k/a)^2 \gg m^2(a)$, the expression for the vertex reduces to $\nu \simeq 4/3$. This is observed in Figure (6.1) as well, where the vertex ν asymptotes to a value of approximately 1.33, indicating an enhancement of the effective gravitational strength, as expected in the presence of linear modifications to gravity [11].

We can also observe that, in the case of a stronger modification to general relativity which correspond to larger values of $|f_{R0}|$, the linear mod-

ification saturates to $\nu \sim 4/3$ at earlier times (and large scales) than in models with a smaller $|f_{R0}|$.

6.1.2 Non-Linear Vertices and High-Curvature Regime

The non-linear vertices ν_2, ν_{22}, and ν_3 encode higher-order corrections to the modified Poisson equation that arise as a result of screening mechanisms. Therefore, they are expected to become dominant only near the transitional regime. Figures (6.2a)-(6.2c) show the second and third order vertices evaluated over the (a, k) plane. As before, the evolution of the Compton crossing is overlaid as a white dashed curve across all the plots.

We would like to remind the reader that the non-linear vertices ν_2, ν_{22}, and ν_3 arise from higher-order interactions that encode the screening mechanisms and not from mode couplings. From Figures (6.2), one can observe that these vertices are only dominant near the Compton crossing, where the transition from the low-curvature to the high-curvature regime takes place. They are negligible at early times, consistent with the predictions of a high-redshift universe, when the modifications to gravity are screened. As discussed in [33], the high-curvature solutions correspond to $R \simeq \kappa^2\rho$, where the field gradients are negligible and general relativity is restored. While the linear vertex controls the overall enhancement of gravitational strength in the unscreened regime, the non-linear vertices are responsible for the restoration of general relativity by suppressing this enhancement near the Compton crossing. This is indeed what is observed across Figures (6.1)-(6.2), since when the linearisation is valid, the solution is low-curvature everywhere [33]. Therefore, the non-linear terms only become dominant when linearisation no longer holds. We also observe that the non-linear vertices exhibit weak scale-dependence at early times.

Compton Crossing and High-Curvature Regime Below the Compton crossing, when $(k/a)^2 \ll m^2(a)$, across Figures (6.1)-(6.2), we can observe that all modifications to gravity are strongly suppressed or screened. Here, the linear vertex satisfies $\nu \sim 1$, while the non-linear contributions ν_2, ν_{22}, and $\nu_3 \sim 0$, which are consistent with their respective GR values. This regime corresponds to the high-curvature solution which is intrinsically non-linear [33].

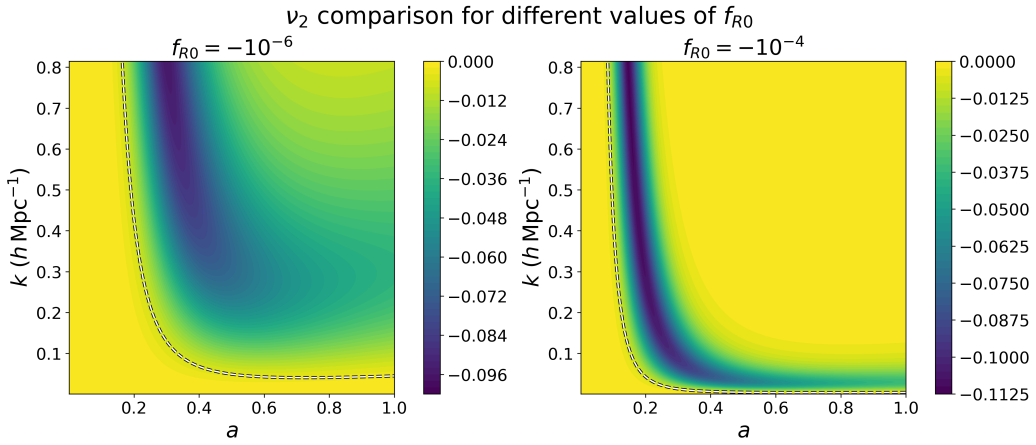

(a) Non-linear vertex $\nu_2(a,k)$ in the Hu-Sawicki model of $f(R)$ gravity.

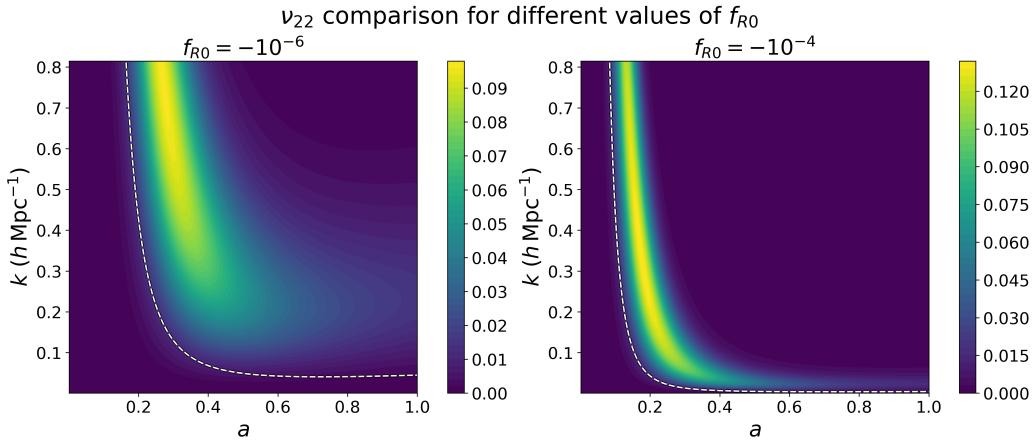

(b) Non-linear vertex $\nu_{22}(a,k)$ in the Hu-Sawicki model of $f(R)$ gravity. This contribution is more localised compared to ν_2, and it peaks closer to the Compton crossing.

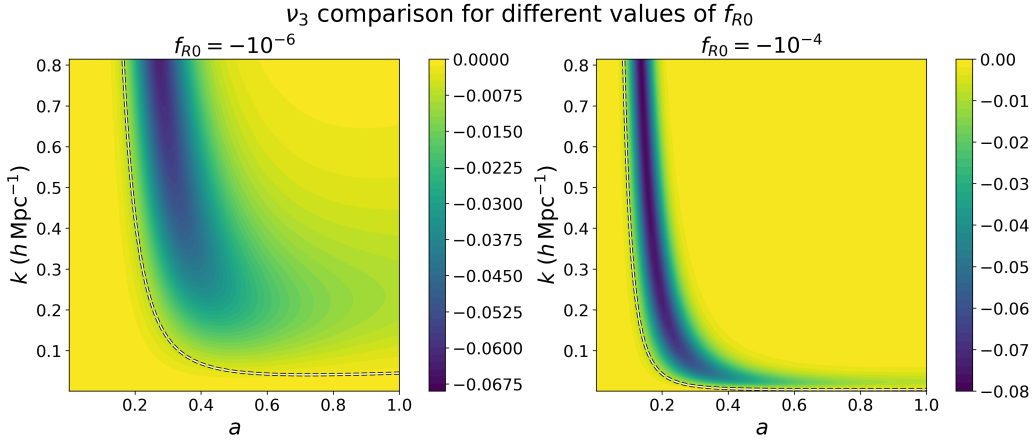

(c) Non-linear vertex $\nu_3(a,k)$ in Hu-Sawicki model of $f(R)$ gravity. It shows a similar structure to ν_{22}, but with a lower amplitude and an opposite sign.

Figure 6.2: Non-linear vertices in Hu–Sawicki $f(R)$ gravity as functions of scale and time, shown for $|f_{R0}| = 10^{-6}$ (left panels) and $|f_{R0}| = 10^{-4}$ (right panels). The dashed curves denote the Compton crossing. Below the crossing, the modifications are strongly suppressed by screening; in the unscreened regime they exhibit a bump-like enhancement before decaying at late times. Across all non-linear vertices, the width of the transitional regime reduces as $|f_{R0}|$ is increased.

Extremities of Non-Linear Vertices It is also useful to analyse the scaling behaviour of the non-linear vertices in the two regimes defined by the magnitudes of physical wavenumber k/a and scalaron mass $m(a)$. It is known that this scaling is mainly controlled by the form of the function $\Pi(a,k)$, which is given by:

$$\Pi(a,k) = \frac{k^2}{a^2} + m^2(a). \tag{6.10}$$

There are two regimes within which the vertices can be studied:

1. **Case I: $\mathbf{k/a \ll m(a)}$**
   In this regime, the expression for the function $\Pi(a,k)$ reduces to $\Pi(a,k) \approx m(a)$. This means that the non-linear vertices would effectively scale as,

   $$\nu_2 \propto \left(\frac{k}{a}\right)^2 \frac{H^2 M_2}{m^6}, \quad \nu_3 \propto \left(\frac{k}{a}\right)^2 \frac{H^4 M_3}{m^8}, \quad \nu_{22} \propto \left(\frac{k}{a}\right)^2 \frac{H^4 M_2 M_2}{m^{10}}. \tag{6.11}$$

   Therefore, we can see that the vertices are strongly suppressed by high powers of mass, and this reflects the fact that the scalaron is heavy in this regime as a consequence of screening.

2. **Case II: $\mathbf{k/a \gg m(a)}$**
   In the opposite limit, the expression for $\Pi(a,k)$ reduces to $\Pi(a,k) \approx (k/a)^2$. In this case, the vertices scale as,

   $$\nu_2 \propto \left(\frac{k}{a}\right)^2 \frac{H^2 M_2}{k^2 k_1^2 k_2^2}, \quad \nu_3 \propto \left(\frac{k}{a}\right)^2 \frac{H^4 M_3}{k^2 k_1^2 k_2^2 k_3^2}, \quad \nu_{22} \propto \left(\frac{k}{a}\right)^2 \frac{H^4 M_2 M_2}{k^2 k_1^2 k_2^2 k_3^2 k_{23}^2} \tag{6.12}$$

   Therefore, in this regime, the vertices decay as inverse powers of the comoving wavenumber k. This scaling shows why the non-linear vertices peak near the Compton crossing and experience a steep fall-off at sufficiently high wavenumbers.

Together, these two limits explain the origin of the localised, bump-like feature of the non-linear vertices. On large scales, they are suppressed due to the large scalaron mass and vanish due to screening, and on very small scales they decay as inverse powers of the wavenumber. Therefore,

the vertices show a significant contribution only in the intermediate transitional regime around the Compton crossing, i.e., when $k/a \sim m(a)$.

6.1.3 Width of Transition Region and Dependence on $|f_{R0}|$

To visualise the onset of the non-linear vertex contributions and to study how they depend on the Hu-Sawicki parameter f_{R0}, we plot the outermost contour for each vertex in the (a, k) plane for three choices of f_{R0}. The transition regime is defined as the band in time and scale over which the non-linear corrections are dominant. This provides a visual measure of how the transition shifts with f_{R0} and how its width changes across vertices.

Figures (6.3a)-(6.3c) show the outermost contours of the non-linear vertices, for three choices of f_{R0}. Two trends can be observed across the three plots,

1. As $|f_{R0}|$ is increased, the transition shifts to earlier times and larger physical scales.
2. As $|f_{R0}|$ is increased, the width of the transition region, where the non-linear contributions are dominant, becomes narrower.

The first trend can be explained by considering the expression for f_{RR}, which in turn enters the definition of the scalar mass. It is known that $f_{RR} \propto |f_{R0}|$. This implies that when $|f_{R0}|$ is increased, f_{RR} increases as well. Since $m_{f_R} \propto f_{RR}^{-1} \propto \lambda_{f_{R0}}^{-1}$, an increase in the parameter $|f_{R0}|$ would imply that the Compton wavelength increases as well. As a consequence, the Compton crossing is shifted to smaller wavenumbers and earlier times, as more Fourier modes satisfy $k \gtrsim am(a)$. This means that more modes lie within the low-curvature regime where linearisation holds. As a result, the linear modification saturates more quickly, leaving a narrow window over which the non-linear effects dominate, which in turn gives rise to the second trend.

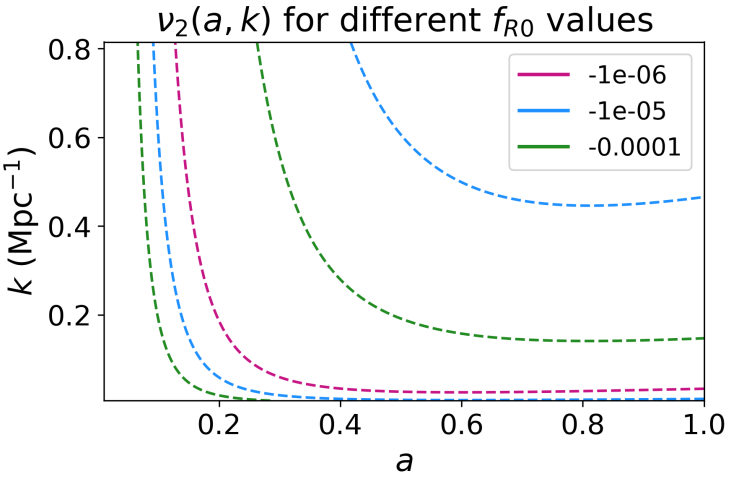

(a) Outermost contour of $\nu_2(a,k)$ for three values of f_{R0}. It displays a comparatively broader transition band compared to ν_{22} and ν_3.

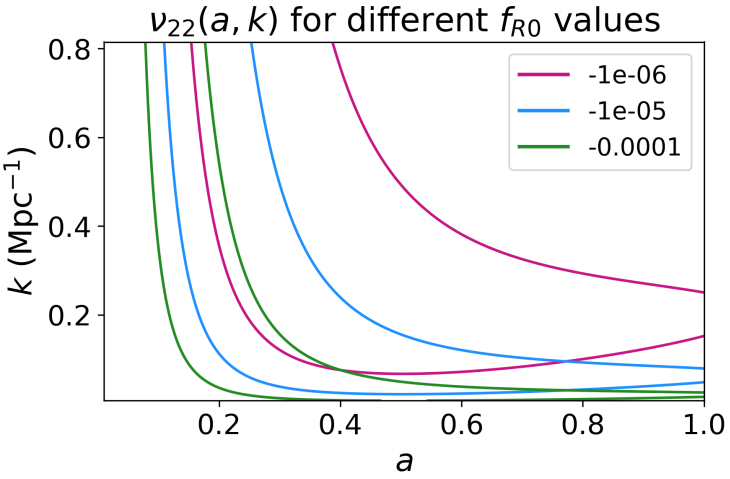

(b) Outermost contour of $\nu_{22}(a,k)$ for three values of f_{R0}. The transition band is the narrowest compared to the other vertices.

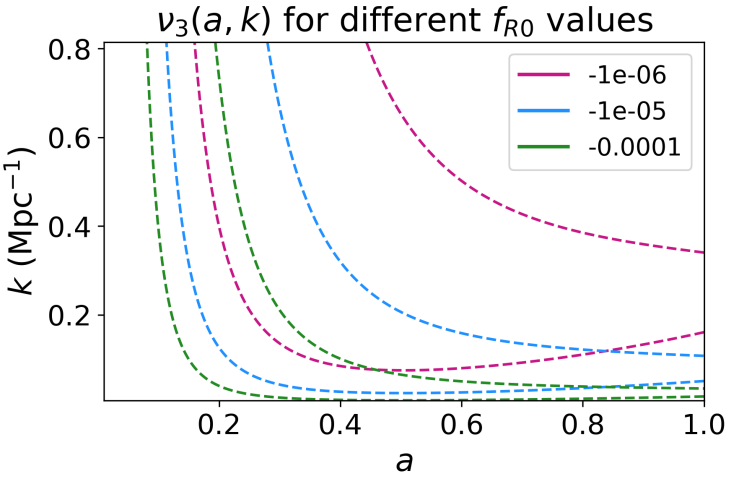

(c) Outermost contour of $\nu_3(a,k)$ for three values of f_{R0}. It exhibits a similar structure to ν_{22} but with an opposite sign.

Figure 6.3: Outermost contours of the Poisson equation vertices in Hu-Sawicki $f(R)$ gravity for $f_{R0} = -10^{-6}, -10^{-5}, -10^{-4}$. For all three vertices, increasing $|f_{R0}|$ reduces the width of the transition regime. This implies that the stronger the deviation from GR, more rapidly does the linear modification saturate.

Chapter 7

Discussion

In this thesis, we studied the scale-dependent modifications to gravity and their implications for non-linear structure formation. We began by examining the fluid description of cold dark matter within the framework of standard perturbation theory and highlighted how non-linear mode couplings arise from the continuity and Euler equations and are encoded within the kernels F_n and G_n. We also saw how these kernels contribute to higher-order corrections to the matter power spectrum in the quasi-non-linear regime. This served as the foundation for studying the evolution of density perturbations when modifications to gravity are introduced.

We then examined the role of the additional scalar degree of freedom that arises when gravity is modified. By perturbing the field equations, we arrived at the modified Poisson equation that, unlike its GR counterpart, contains a scale-dependent linear correction and non-linear source terms. These modifications directly propagate into the Euler equation and consequently into the mode-coupling kernels that govern non-linear growth.

We also studied screening mechanisms, specifically chameleon screening, and how it allows such theories to evade the stringent bounds from local tests of gravity. In particular, we explored the dynamics responsible for suppressing the scalar degree of freedom in high-density regions like the solar system and restoring gravity. This was achieved by an effective potential with a density-dependent minimum. This ensured that in regions of high density, the scalar field acquired a larger effective mass, which suppressed the range of the fifth force it mediates. This screening mechanism manifests itself in the structure of the interaction coefficients M_1, M_2, M_3, and the scale-dependent function $\Pi(a, k)$, which enter the

modified Poisson equation. We then specialised this analysis to consider $f(R)$ gravity. Using sub-horizon quasi-static approximations, we derived the explicit forms of the interaction coefficients in the Hu-Sawicki model. These coefficients encode information about both the background cosmic expansion (ΛCDM) as well as the non-linear self-interactions of the scalar field.

The numerical analysis of these vertices provided further insight into their scale and time dependence. It was seen that at early times, when the universe was in a high-curvature state, the modifications to gravity were suppressed and GR was restored. At late times, we could observe these modifications emerge as the interaction vertices departed from their GR values. However, the non-linear vertices were only dominant in the vicinity of the Compton crossing, since at this stage they encode screening effects. This meant that in regions where linearisation holds, the non-linear vertices were not active. We also observed how these vertices decay as inverse powers of the comoving wavenumber k. This explained why their contributions were localised to a narrow band in scale and time. The width and location of the transition regime depended on parameter f_{R0}, and as $|f_{R0}|$ was increased, the linear modification saturated more quickly and a narrower transition band was observed. Lastly, we note that at this stage it is not prudent to comment on the nature of the non-linear matter power spectrum, as this requires solving a closed system of fluid equations with scale-dependent couplings, which is not a trivial task. The present analysis instead focuses on the structure of the interaction vertices which make up the basic ingredients for such a computation.

Given the precision era of Stage IV surveys like *Euclid*, it is important to develop the theoretical framework to interpret data from the quasi-non linear and non-linear regimes of structure formation. These results highlight the importance of incorporating non-linear corrections and screening effects when modeling structure formation in modified gravity. While linear modifications capture the scale-dependence of the theory, they do not include screening effects, which only emerge in higher-order interactions.

The next step would be to derive the explicit forms of the modified kernels F_n and G_n in case of Hu-Sawicki $f(R)$ theory and subsequently compute the loop corrections to the matter power spectrum. This would allow for more direct comparison against results from observations or N-body simulations. The methodology discussed in this thesis is not restricted to $f(R)$ models. Therefore, it may be productive to apply a similar analysis to other modified gravity models with their own characteristic screening mechanisms in the future.

Appendix A

Code

The full Python notebook for plotting the modified Poisson equation vertices is available here.

Bibliography

[1] E. J. Copeland, M. Sami, and S. Tsujikawa, *Dynamics of Dark Energy*, International Journal of Modern Physics D **15**, 1753 (2006).

[2] T. Clifton, P. G. Ferreira, A. Padilla, and C. Skordis, *Modified Gravity and Cosmology*, Phys. Rept. **513**, 1 (2012).

[3] P. Brax and P. Valageas, *Structure Formation in Modified Gravity Scenarios*, Physical Review D **86**, 063512 (2012).

[4] S. Weinberg, *Photons and Gravitons in Perturbation Theory: Derivation of Maxwell's and Einstein's Equations*, Physical Review **138**, B988 (1965).

[5] P. Brax, C. van de Bruck, A.-C. Davis, J. Khoury, and A. Weltman, *Detecting Dark Energy in Orbit — The Cosmological Chameleon*, Physical Review D **70**, 123518 (2004).

[6] P. Brax, C. van de Bruck, A.-C. Davis, and A. M. Green, *Small Scale Structure Formation in Chameleon Cosmology*, Physics Letters B **633**, 441 (2006).

[7] J. Khoury and A. Weltman, *Chameleon Cosmology*, Physical Review D **69**, 044026 (2004).

[8] B. Bertotti, L. Iess, and P. Tortora, *A Test of General Relativity Using Radio Links with the Cassini Spacecraft*, Nature **425**, 374 (2003).

[9] C. D. Hoyle, D. J. Kapner, B. R. Heckel, E. G. Adelberger, J. H. Gundlach, U. Schmidt, and H. E. Swanson, *Sub-millimeter Tests of the Gravitational Inverse-square Law*, Physical Review D **70**, 042004 (2004).

[10] I. Achitouv, M. Baldi, E. Puchwein, and J. Weller, *Imprint of $f(R)$ gravity on nonlinear structure formation*, Phys. Rev. D **93**, 103522 (2016).

[11] L. Pogosian and A. Silvestri, *Erratum: Pattern of growth in viable $f(R)$ cosmologies*, Physical Review D **81**, 049901 (2010).

[12] J. Adamek et al., *Euclid preparation - LXII. Simulations and non-linearities beyond Lambda cold dark matter. 1. Numerical methods and validation*, Astron. Astrophys. **695**, A230 (2025).

[13] N. Frusciante et al., *Euclid preparation. Review of forecast constraints on dark energy and modified gravity*, (2025).

[14] C. Pichon and F. Bernardeau, *Vorticity generation in large-scale structure caustics*, Astronomy and Astrophysics **343**, 663 (1999).

[15] V. Assassi, D. Baumann, D. Green, and E. Pajer, *Effective theory of large-scale structure with primordial non-Gaussianity*, Journal of Cosmology and Astroparticle Physics **2015**, 024 (2015).

[16] J. N. Fry and C.-P. Ma, *The Onset of Nonlinearity in Cosmological Structure*, Annals of the New York Academy of Sciences **927**, 143 (2001).

[17] M. H. Goroff, B. Grinstein, S.-J. Rey, and M. B. Wise, *Coupling of Modes of Cosmological Mass Density Fluctuations*, The Astrophysical Journal **311**, 6 (1986).

[18] M. Crocce and R. Scoccimarro, *Renormalized Cosmological Perturbation Theory*, Physical Review D **73**, 063519 (2006).

[19] R. J. Adler, B. Casey, and O. C. Jacob, *Vacuum Catastrophe: An Elementary Exposition of the Cosmological Constant Problem*, American Journal of Physics **63**, 620 (1995).

[20] G. R. Bengochea, G. León, E. Okon, and D. Sudarsky, *Can the Quantum Vacuum Fluctuations Really Solve the Cosmological Constant Problem?*, The European Physical Journal C **80**, 18 (2020).

[21] A. Shomer, *A Pedagogical explanation for the non-renormalizability of gravity*, (2007).

[22] S. M. Carroll, *Spacetime and Geometry: An Introduction to General Relativity*, Cambridge University Press, 2019.

[23] C. M. Will, *The Confrontation between General Relativity and Experiment*, Living Reviews in Relativity **9** (2006).

[24] G. Dvali and M. Zaldarriaga, *Changing α with Time: Implications for Fifth-Force-Type Experiments and Quintessence*, Physical Review Letters **88**, 091303 (2002).

[25] C. M. Will, *Theory and Experiment in Gravitational Physics*, Cambridge University Press, Cambridge, 2 edition, 2018.

[26] A. A. Starobinsky, *Spectrum of relict gravitational radiation and the early state of the universe*, JETP Letters **30**, 682 (1979), [Pisma Zh. Eksp. Teor. Fiz. 30, 719 (1979)].

[27] B. Whitt, *Fourth Order Gravity as General Relativity Plus Matter*, Phys. Lett. B **145**, 176 (1984).

[28] A. D. Dolgov and M. Kawasaki, *Can modified gravity explain accelerated cosmic expansion?*, Physics Letters B **573**, 1 (2003).

[29] Á. Núñez and S. Solganik, *Ghost Constraints on Modified Gravity*, Physics Letters B **608**, 189 (2005).

[30] H. Nariai, *Gravitational Instability of Regular Model-Universes in a Modified Theory of General Relativity*, Progress of Theoretical Physics **49**, 165 (1973).

[31] V. T. Gurovich and A. A. Starobinsky, *QUANTUM EFFECTS AND REGULAR COSMOLOGICAL MODELS*, Sov. Phys. JETP **50**, 844 (1979).

[32] K. Koyama, A. Taruya, and T. Hiramatsu, *Nonlinear evolution of the matter power spectrum in modified theories of gravity*, Physical Review D **79**, 123512 (2009).

[33] W. Hu and I. Sawicki, *Models of f(R) Cosmic Acceleration*, Physical Review D **76**, 064004 (2007).

[34] Y.-S. Song, W. Hu, and I. Sawicki, *The large scale structure of $f(R)$ gravity*, Physical Review D **75**, 044004 (2007).

[35] P. Collaboration et al., *Planck 2018 results. VI. Cosmological parameters*, Astronomy & Astrophysics **641**, A6 (2020).

[36] L. Piga, M. Marinucci, G. D'Amico, M. Pietroni, F. Vernizzi, and B. S. Wright, *Constraints on Modified Gravity from the BOSS Galaxy Survey*, Journal of Cosmology and Astroparticle Physics **2023**, 038 (2023).

[37] I. Sawicki and W. Hu, *Stability of Cosmological Solution in $f(R)$ Models of Gravity*, Physical Review D **98**, 083528 (2018).

[38] P. Zhang, *Testing Gravity Against the Early Time Integrated Sachs–Wolfe Effect*, Physical Review D **73**, 123504 (2006).